



# Synthesis, characterization, HSA/DNA interactions and antitumor activity of new $[\text{Ru}(\eta^6\text{-p-cymene})\text{Cl}_2(\text{L})]$ complexes

Maja B. Đukić<sup>a</sup>, Marija S. Jeremić<sup>a</sup>, Ignjat P. Filipović<sup>a</sup>, Olivera R. Klisurić<sup>b</sup>, Vesna V. Kojić<sup>c</sup>,  
Dimitar S. Jakimov<sup>c</sup>, Ratimir M. Jelić<sup>d</sup>, Valentina Onnis<sup>e</sup>, Zoran D. Matović<sup>a,\*</sup>

<sup>a</sup> University of Kragujevac, Faculty of Science, Department of Chemistry, Radoja Domanovića 12, 34000 Kragujevac, Serbia

<sup>b</sup> University of Novi Sad, Faculty of Sciences, Department of Physics, Trg Dositeja Obradovića 4, 21000 Novi Sad, Serbia

<sup>c</sup> Oncology Institute of Vojvodina, Faculty of Medicine, University of Novi Sad, Put Doktora Goldmana 4, 21204 Sremska Kamenica, Serbia

<sup>d</sup> University of Kragujevac, Faculty of Medical Sciences, Department of Pharmacy, Svetozara Markovića 69, 34000 Kragujevac, Serbia

<sup>e</sup> Department of Life and Environmental Sciences, Unit of Pharmaceutical, Pharmacological and Nutraceutical Sciences, University of Cagliari, University Campus, S.P. n° 8, Km 0.700, I-09042 Monserrato (CA), Italy

## ARTICLE INFO

### Keywords:

Ruthenium(II) complexes  
HSA interactions  
DNA interactions  
Molecular docking  
Antiproliferation

## ABSTRACT

Three new ruthenium(II) complexes were synthesized from different substituted isothiazole ligands 5-(methylamino)-3-pyrrolidine-1-ylisothiazole-4-carbonitrile (1), 5-(methylamino)-3-(4-methylpiperazine-1-yl)isothiazole-4-carbonitrile (2) and 5-(methylamino)-3-morpholine-4-ylisothiazole-4-carbonitrile (3):  $[\text{Ru}(\eta^6\text{-p-cymene})\text{Cl}_2(\text{L1})]\cdot\text{H}_2\text{O}$  (4),  $[\text{Ru}(\eta^6\text{-p-cymene})\text{Cl}_2(\text{L2})]$  (5) and  $[\text{Ru}(\eta^6\text{-p-cymene})\text{Cl}_2(\text{L3})]$  (6). All complexes were characterized by IR, UV–Vis, NMR spectroscopy, and elemental analysis. The molecular structures of all ligands and complexes 4 and 6 were determined by an X-ray. The results of the interactions of CT-DNA (calf thymus deoxyribonucleic acid) and HSA (human serum albumin) with ruthenium (II) complexes reveal that complex 4 binds well to CT-DNA and HSA. Kinetic and thermodynamic parameters for the reaction between complex and HSA confirmed the associative mode of interaction. The results of Quantum mechanics (QM) modelling and docking experiments toward DNA dodecamer and HSA support the strongest binding of the complex 4 to DNA major groove, as well as its binding to IIA domain of HSA with the lowest  $\Delta G$  energy, which agrees with the solution studies. The modified GOLD docking results are indicative for  $\text{Ru}(\text{p-cymene})\text{LCl}-(\text{HSA-GLU292})$  binding and GOLD/MOPAC(QM) docking/modelling of DNA/Ligand ( $\text{Ru}(\text{II})\text{-N(7)dG7}$ ) covalent binding. The cytotoxic activity of compounds was evaluated by MTT (3-(4,5-dimethyl-2-thiazolyl)-2,5-diphenyl-2H-tetrazolium bromide) assay. Neither of the tested compounds shows activity against a healthy MRC-5 cell line while the MCF-7 cell line is the most sensitive to all. Compounds 3, 4 and 5 were about two times more active than cisplatin, while the antiproliferative activity of 6 was almost the same as with cisplatin. Flow cytometry analysis showed the apoptotic death of the cells with a cell cycle arrest in the subG1 phase.

## 1. Introduction

A significant contribution to the fight against malignancy was achieved using transition metal complexes. Probably the most significant among them is cisplatin, which has been used with more or less success for more than half a century [1]. Although efficient against the number of cancers, cisplatin also causes severe side-effects, which leads to e.g. peripheral neuropathy, hair loss, and myelotoxicity in patients [2]. Furthermore, for decades, chemists have been persistently working on the synthesis of new potentially bio-active metal complexes, changing either the structure of the ligand or the nature of the metal ion (Ru, Os, Fe, Cu ...). Ruthenium is very often seen in complexes with a

specific activity toward metastatic cancer cells. The reader may find more relevant intro about the anticancer activity of half-sandwich ruthenium(II) complexes in many reviews and papers in which the synthesis and the mechanisms of its action were reported [3–6]. Also, Ru(III) complexes such as NAMI-A ( $(\text{ImH})[\text{trans-RuCl}_4(\text{dmsO-S})(\text{Im})]$ , Im = imidazole) and KP1019 ( $(\text{IndH})[\text{trans-RuCl}_4(\text{Ind})_2]$ , Ind = indazole) have undergone phase I of a clinical trial [7] (Fig. 1). Nevertheless, half-sandwich piano stool Ru(II) complexes have attracted greater interest in recent years for their antimetastatic and anticancer properties. RAPTA-C ( $[\text{Ru}(\eta^6\text{-p-cymene})(\text{PTA})\text{Cl}_2]$ , where PTA = 1,3,5-triaza-7-phosphaadamantane) [8] is anti-metastatic and anti-angiogenic agent able to form adducts with histone proteins [9].

\* Corresponding author.

E-mail address: [zmatovic@kg.ac.rs](mailto:zmatovic@kg.ac.rs) (Z.D. Matović).

<https://doi.org/10.1016/j.jinorgbio.2020.111256>

Received 23 July 2020; Received in revised form 8 September 2020; Accepted 10 September 2020

Available online 15 September 2020

0162-0134/ © 2020 Elsevier Inc. All rights reserved.

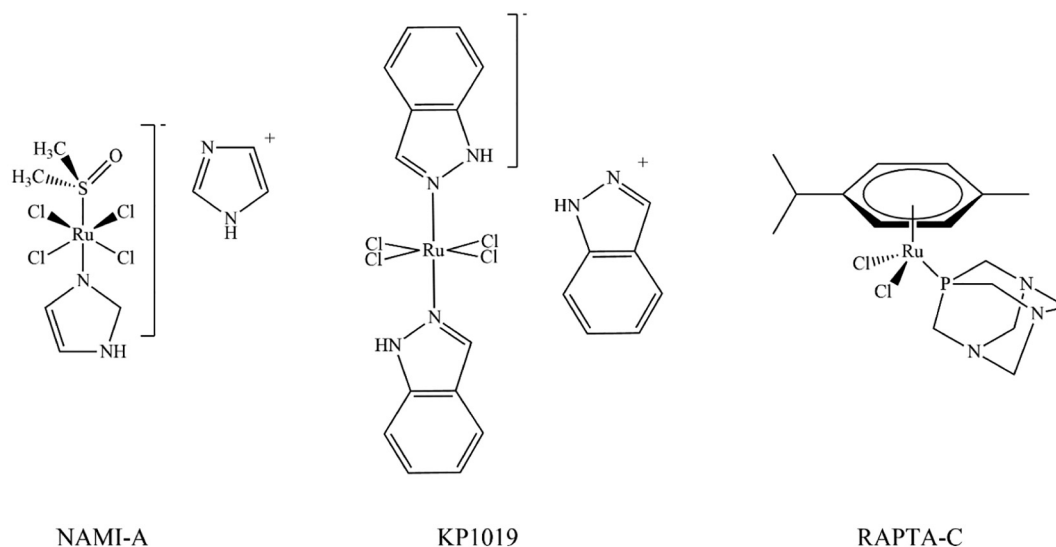


Fig. 1. Ruthenium(III) and ruthenium(II) arene complexes currently in clinical trials.

Encouraged by these results, many research groups have based their research on the synthesis of ruthenium(II) complexes, which will show greater activity against malignant cells and less toxicity to healthy cells. Thus, Romerosa et al. synthesized a large number of ruthenium complexes with different ligands:  $[\text{RuCp}(\text{PPh}_3)_2(\text{HdmoPTA})](\text{OSO}_2\text{CF}_3)_2$  ( $\text{HdmoPTA} = 3,7\text{-H-}3,7\text{-dimethyl-}1,3,7\text{-triazol-}5\text{-phosphabicyclo[3.3.1]nonane}$ ) [10],  $[\text{RuCp}(\text{PPh}_3)_2\text{-}\mu\text{-dmoPTA-}1\kappa\text{P:}2\kappa^2\text{N,N'-CoCl}_2](\text{OTf})\cdot 0.25\text{H}_2\text{O}$  ( $\text{OTf} = \text{trifluoromethanesulfonate}$ , i.e.  $\text{CF}_3\text{SO}_3$ ) [11], bimetallic Ru–Zn complex  $[\text{RuCp}(\text{PPh}_3)_2\text{-}\mu\text{-dmoPTA-}1\kappa\text{P:}2\kappa^2\text{N,N'-ZnCl}_2](\text{CF}_3\text{SO}_3)$  [12] etc.... Such complexes are generally insoluble or sparingly soluble in water. Similar antitumor active ruthenium(II) complexes were summarized in review articles [13]. On the other hand, data on the antitumor activity of metal complexes with isothiazoles are very scarce. The mechanism of action of these ruthenium(III) compounds involves at least their interaction with serum proteins such as albumin and transferrin that endows them with tumor seeking properties [14]; second, ruthenium(III) complexes appear to be activated through intracellular reduction to allow generation of toxic ruthenium(II) species [15,16]; and third, at the tumor site reactions (binding) with proteins are preferred to DNA binding, which contrasts with the behavior of platinum(II) complexes such as cisplatin [17–19]. Reaction rates between Ru-*p*-cymene and human serum albumin (HSA) coordinating ligands are strongly affected by the type of the donor atoms. Complex formation with (O,O) or (O,O,O) donor ligands is a fast process at physiological pH, while (N) and (N, N, N) donor ligands chelate the Ru-*p*-cymene rather slowly (hours to days) [20–23]. Therefore metalation of important serum proteins by ruthenium(II) appears to be probable and should be caused by the nature of the ruthenium drugs [24].

Multidonor heterocyclic ligands demonstrate different and diverse capabilities for the coordination of various metal ions. The electron-rich polyfunctional derivatives of thiazole and isothiazole belong to this type of ligand, and their bioactive coordinating compounds have attracted significant attention in medicine and pharmacy [25–27]. Basically, the thiazole heterocyclic ring can be found in two isomeric forms, 1,3-thiazole (known as thiazole) and 1,2-thiazole (known as isothiazole). They showed a wide range of useful properties which led researchers to study the synthesis and chemical transformations of its derivatives [28–30]. Some of them have shown effectiveness in the treatment of Alzheimer's disease, where their effects are based on inhibition of serine protease, on anti-inflammation and anticonvulsion [31]. Also, these types of compounds show great antiviral activity and inflammatory properties [32–34]. Besides their role in the synthesis of

biologically active substances, isothiazoles can serve as ligands for transition metal complexes [31,35–38].

Recently, we published the results of our research on syntheses and biology of  $[\text{Ru}(\eta^6\text{-p-cymene})(\text{R-imidazole})\text{Xn}]^{2-n}$  complexes [39]. Following our work on heterocycles and half-sandwich ruthenium(II) complexes, we describe here the synthesis, characterization and crystal structures of some isothiazole ligands and corresponding ruthenium(II) complexes. Also, the results of their cytotoxicity against four cancer cell lines and one non-cancer cell in vitro have been reported. Additionally, we examined the in vitro interaction of the complexes with calf thymus deoxyribonucleic acid (CT-DNA), as well as the in vitro affinity of the complexes for human serum albumin by UV–Vis spectroscopy and fluorescence emission spectroscopy as well as the in vitro interaction of the complexes with CT-DNA. Furthermore, quantum mechanics modelling and docking simulations toward DNA dodecamer and HSA have been done. AutoDock and Vina have been used with new parameters for ruthenium(II) as well as modified GOLD software in order to establish binding energies of the Ligand–HSA(DNA) system.

## 2. Experimental

### 2.1. Materials and physical measurements

$[\text{Ru}(\eta^6\text{-p-cymene})\text{Cl}_2]_2$ , ethyl acetate, toluene, dichloromethane, methanol, NaOH, HCl, NaCl, Tris-HCl, highly polymerized CT-DNA and ethidium bromide were purchased from Sigma-Aldrich, used as received.

The stock DNA solution was prepared by diluting CT-DNA with a buffer solution (10 mM tris(hydroxymethyl)-aminomethane (Tris-HCl) and 150 mM NaCl to pH 7.4), after which it was stirred at 4 °C for 3 days, and kept at 4 °C for no longer than a week. The concentration of CT-DNA in stock solution was determined by UV absorption at 260 nm using a molar absorption coefficient ( $\epsilon_{260} = 6600 \text{ M}^{-1} \text{ cm}^{-1}$ ) [40]. The purity of the DNA was checked by monitoring the ratio of the absorbance at 260 nm to that at 280 nm. The solution gave a ratio of  $> 1.8$  at  $A_{260}/A_{280}$ , which indicates that DNA was adequately free from protein [41]. Due to the limited solubility of the ligands and metal complexes in the water, stock solutions were prepared by dissolving the compound in DMSO. By diluting the stock solution with buffer (10 mM Tris-HCl and 150 mM NaCl at pH 7.4), working solutions were obtained in which the final concentration of DMSO was at most 8%. Doubly distilled water was used for the preparation of all solutions.

UV–Vis spectra were recorded on a double beam UV–Vis

spectrophotometer model Cary 300 (Agilent Technologies, Santa Clara, USA) with 1.0 cm quartz cells. Emission measurements were carried out using an RF-1501 PC spectrofluorometer (Shimadzu, Japan). The excitation wavelength was fixed, and the emission range was adjusted before measurements, with the excitation and emission slit widths set at 10 nm. All the measurements were conducted in buffer containing Tris-HCl (10 mM) and NaCl (150 mM) and adjusted to pH 7.4 with hydrochloric acid, at 25 °C.

Elemental microanalyses for C, H, N were performed at the Microanalytical laboratory, Faculty of Chemistry, University of Belgrade, Serbia. IR spectra in the 400–4000 cm<sup>-1</sup> region were recorded on a Perkin-Elmer FT-IR spectrophotometer Spectrum One, using the KBr pellets technique. <sup>1</sup>H and <sup>13</sup>C{<sup>1</sup>H} NMR spectra were recorded on a Varian Gemini 2000 spectrometer (200 MHz). Chemical shifts are expressed as  $\delta$  values (ppm) relative to Tetramethylsilane (TMS) as an internal standard. Electronic absorption spectra were recorded on a double beam UV-Vis spectrophotometer model Cary 300 (Agilent Technologies, Santa Clara, USA) with 1.0 cm quartz cells. Kinetic measurements were performed on UV-Vis Perkin-Elmer Lambda 35 double beam spectrophotometer with water thermostated 1.0 cm path-length quartz cuvettes (3.0 mL). Melting points were measured by the Stuart melting device with accuracy  $\pm 1$  °C. Molar conductivities were measured at room temperature on a digital conductivity-meter Crison Multimetre MM 41. The concentration of the solutions of complexes 4–6 in DMSO used for conductivity measurements was  $1 \times 10^{-3}$  M.

## 2.2. Synthesis of compounds

### 2.2.1. Synthesis of ligands (1, 2, 3)

The ligands 5-(methylamino)-3-pyrrolidine-1-ylisothiazole-4-carbonitrile (1), 5-(methylamino)-3-(4-methylpiperazine-1-yl)isothiazole-4-carbonitrile (2) and 5-(methylamino)-3-morpholine-4-ylisothiazole-4-carbonitrile (3) were prepared by the previously reported procedures [42,43]. Herein, we have provided the synthesis of ligand 1 as an example: the ice-cooled solution of 3-amino-2-(methylthiocarbonyl)-3-pyrrolidino-2-propenenitrile (1.05 g, 5 mmol) in anhydrous CHCl<sub>3</sub> (50 mL) was mixed with Br<sub>2</sub> (0.8 g, 5 mmol) and the resulting mixture was stirred for 1 h. The mixture was washed with a solution of NaOH and water. The ligand 1 was obtained by recrystallization from cyclohexane.

### 2.2.2. Synthesis of [Ru( $\eta^6$ -p-cymene)Cl<sub>2</sub>(L1)]·H<sub>2</sub>O (4)

The [Ru( $\eta^6$ -p-cymene)Cl<sub>2</sub>(L1)]·H<sub>2</sub>O was synthesized by following the method described elsewhere [44]. A mixture of [Ru( $\eta^6$ -p-cymene)Cl<sub>2</sub>]<sub>2</sub> (0.0998 g; 0.163 mmol) and ligand 1 (0.2082 g; 1 mmol; 6.1 equiv.) in toluene (15 mL) was refluxed for 3 h (110 °C), cooled and filtered. The solution was evaporated to a volume of ~5 mL at room temperature. Crystals suitable for X-ray crystal analysis were obtained by the addition of ethyl acetate (0.228 g, 42.84%). Melting point = 174 °C. Anal. Cal. for C<sub>19</sub>H<sub>28</sub>Cl<sub>2</sub>N<sub>4</sub>ORuS (Mw = 532.48) C: 42.86, H: 5.30, N: 10.52; found: C: 43.03, H: 5.51, N: 10.78. <sup>1</sup>H NMR (200 MHz, CDCl<sub>3</sub>):  $\delta$ (ppm) 1.35 (d, 6H, CH<sub>3</sub>), 1.82 (s, 3H, 4-CH<sub>3</sub>), 1.95 (qui, 3'-H, 4'-H), 2.31 (s, 3H, 1''-CH<sub>3</sub>), 2.92 (sept, 1H, 1-CH(CH<sub>3</sub>)<sub>2</sub>), 3.58 (t, 5'-H, 2'-H), 5.38 (d, 2H, 2-H, 6-H), 5.60 (d, 2H, 3-H, 5-H) (Fig. S1, ESI). <sup>13</sup>C{<sup>1</sup>H} NMR (50 MHz, CDCl<sub>3</sub>):  $\delta$ (ppm) 19.12 (-CH<sub>3</sub>), 22.42 (1-CH(CH<sub>3</sub>)<sub>2</sub>), 25.56 (C-3', C-4'), 31.38 (C-1''), 33.14 (1-CH(CH<sub>3</sub>)<sub>2</sub>), 48.25 (C-5', C-2'), 80.59 (C-1'''), 81.50 (C-1<sup>IV</sup>), 83.35 (C-2''), 96.82 (C-2, C-6), 98.86 (C-3, C-5), 101.26 (C-4), 102.85 (C-1) (Fig. S2, ESI). IR (KBr, pellet):  $\nu$  (cm<sup>-1</sup>) 3407 ( $\nu$  = CH), 2959, 2925 ( $\nu$ CH), 2235 ( $\nu$ C  $\equiv$  N), 1580, 1524 ( $\nu$ C = C) (Fig. S3, ESI). UV-Vis (CH<sub>3</sub>OH, C =  $2 \times 10^{-3}$  M):  $\lambda_{\text{max/nm}}$  ( $\epsilon$ /L mol<sup>-1</sup> cm<sup>-1</sup>): 342 (sh) (1000), 428 (564) (Fig. S4, ESI).  $\Lambda_{\text{M}}$  (DMSO): 0.01  $\Omega^{-1}$  cm<sup>2</sup> mol<sup>-1</sup>.

### 2.2.3. Synthesis of [Ru( $\eta^6$ -p-cymene)Cl<sub>2</sub>(L2)] (5)

The [Ru( $\eta^6$ -p-cymene)Cl<sub>2</sub>(L2)] was synthesized by following the

method described elsewhere [44] with little modification. A mixture of [Ru( $\eta^6$ -p-cymene)Cl<sub>2</sub>]<sub>2</sub> (0.0998 g; 0.163 mmol) and ligand 2 (0.2373 g; 1 mmol; 6.1 equiv.) in dichloromethane (15 mL) was refluxed for 3 h (39 °C), cooled and filtered. The solution was evaporated to a volume of ~5 mL at room temperature. After a few days, the precipitate was filtered, yielding a green powdery residue. This complex was washed with diethyl ether and air-dried (0.192 g, 35.52%). Melting point = 137 °C. Anal. Cal. for C<sub>20</sub>H<sub>29</sub>Cl<sub>2</sub>N<sub>5</sub>RuS (Mw = 543.52) C: 44.20, H: 5.38, N: 12.89; found: C: 44.09, H: 5.33, N: 12.65. <sup>1</sup>H NMR (200 MHz, CDCl<sub>3</sub>):  $\delta$ (ppm) 1.36 (d, 6H, CH<sub>3</sub>), 2.21 (s, 3H, 4-CH<sub>3</sub>), 2.33 (s, 3H, 1''-CH<sub>3</sub>), 2.51 (t, 3'-H, 5'-H), 2.81 (sept, 1H, 1-CH(CH<sub>3</sub>)<sub>2</sub>), 2.99 (s, 3H, 1''-CH<sub>3</sub>), 3.58 (t, 2'-H, 6'-H), 5.40 (d, 2H, 2-H, 6-H), 5.62 (d, 2H, 3-H, 5-H) (Fig. S5, ESI). <sup>13</sup>C{<sup>1</sup>H} NMR (50 MHz, CDCl<sub>3</sub>):  $\delta$ (ppm) 19.15 (-CH<sub>3</sub>), 22.34 (1-CH(CH<sub>3</sub>)<sub>2</sub>), 31.36 (C-1''), 33.22 (1-CH(CH<sub>3</sub>)<sub>2</sub>), 46.10 (C-1<sup>V</sup>), 47.50 (C-2', C-6'), 54.61 (C-3', C-5'), 87.49 (C-1'''), 97.94 (C-1<sup>IV</sup>), 115.35 (C-2, C-6), 117.20 (C-3, C-5), 135.50 (C-4), 136.38 (C-1), 159.65 (C-5''), 164.34 (C-2'') (Fig. S6, ESI). IR (KBr, pellet):  $\nu$  (cm<sup>-1</sup>) 3266 ( $\nu$  = CH), 2961, 2935 ( $\nu$ CH), 2239, 2200 ( $\nu$ C  $\equiv$  N), 1565 ( $\nu$ C = C) (Fig. S7, ESI). UV-Vis (CH<sub>3</sub>OH, C =  $2 \times 10^{-3}$  M):  $\lambda_{\text{max/nm}}$  ( $\epsilon$ /L mol<sup>-1</sup> cm<sup>-1</sup>): 390 (sh) (406) (Fig. S4, ESI).  $\Lambda_{\text{M}}$  (DMSO): 0.01  $\Omega^{-1}$  cm<sup>2</sup> mol<sup>-1</sup>.

### 2.2.4. Synthesis of [Ru( $\eta^6$ -p-cymene)Cl<sub>2</sub>(L3)] (6)

The [Ru( $\eta^6$ -p-cymene)Cl<sub>2</sub>(L3)] was synthesized by following the method described elsewhere [44]. A mixture of [Ru( $\eta^6$ -p-cymene)Cl<sub>2</sub>]<sub>2</sub> (0.0998 g; 0.163 mmol) and ligand 3 (0.2242 g; 1 mmol; 6.1 equiv.) in toluene (15 mL) was refluxed for 3 h (110 °C) and cooled. The orange crystals were obtained from the toluene (0.255 g, 48.06%). Melting point = 216 °C. Anal. Cal. for C<sub>19</sub>H<sub>26</sub>Cl<sub>2</sub>N<sub>4</sub>ORuS (Mw = 530.47) C: 43.02, H: 4.94, N: 10.56; found: C: 43.31, H: 4.92, N: 10.46. <sup>1</sup>H NMR (200 MHz, CDCl<sub>3</sub>):  $\delta$ (ppm) 1.36 (d, 6H, CH<sub>3</sub>), 2.16 (s, 3H, 1''-CH<sub>3</sub>), 2.32 (s, 3H, 4-CH<sub>3</sub>), 2.92 (sept, 1H, 1-CH(CH<sub>3</sub>)<sub>2</sub>), 3.50 (t, 2'-H, 6'-H), 3.78 (t, 5'-H, 3'-H), 5.41 (d, 2H, 2-H, 6-H), 5.62 (d, 2H, 3-H, 5-H) (Fig. S8, ESI). <sup>13</sup>C{<sup>1</sup>H} NMR (50 MHz, CDCl<sub>3</sub>):  $\delta$ (ppm) 19.09 (-CH<sub>3</sub>), 22.42 (1-CH(CH<sub>3</sub>)<sub>2</sub>), 31.38 (C-1''), 33.23 (1-CH(CH<sub>3</sub>)<sub>2</sub>), 48.00 (C-2', C-6'), 66.42 (C-3', C-5'), 80.59 (C-1'''), 83.45 (C-1<sup>IV</sup>), 96.75 (C-2, C-6), 98.97 (C-3, C-5), 101.26 (C-4), 102.84 (C-1), 128.16 (C-5''), 128.97 (C-2'') (Fig. S9, ESI). IR (KBr, pellet):  $\nu$  (cm<sup>-1</sup>) 3432 ( $\nu$  = CH), 2969, 2923 ( $\nu$ CH), 2228 ( $\nu$ C  $\equiv$  N), 1567 ( $\nu$ C = C) (Fig. S10, ESI). UV-Vis (CH<sub>3</sub>OH, C =  $2 \times 10^{-3}$  M):  $\lambda_{\text{max/nm}}$  ( $\epsilon$ /L mol<sup>-1</sup> cm<sup>-1</sup>): 337 (1118) and 430 (654) (Fig. S4, ESI).  $\Lambda_{\text{M}}$  (DMSO): 0.01  $\Omega^{-1}$  cm<sup>2</sup> mol<sup>-1</sup>.

## 2.3. Crystal structure determination

Single crystals of complexes 4, 6 and ligands 1, 2 and 3 were mounted on a glass fiber and crystallographic data were collected using the Rigaku (Oxford Diffraction) Gemini S diffractometer with a CCD area detector ( $\lambda_{\text{MoK}\alpha}$  = 0.71073 Å, monochromator: graphite) at 293 K. CrysAlisPro and CrysAlis RED software packages [45] were used for data collection and data integration. Analysis of the integrated data did not reveal any decay. Collected data were corrected for absorption effects by using a Numerical absorption correction based on Gaussian integration over a multifaceted crystal model [46] for compound 4 and analytical numeric absorption correction applying a multifaceted crystal model [47] for compound 6, while collected data for ligands 1, 2 and 3 were corrected for absorption effects by using a Multi-scan absorption correction [48]. Structure solution and refinement were carried out with the programs SHELXT and SHELXL-2014/6 respectively [49]. All calculations were performed using PLATON [50] while MERCURY [51] was employed for molecular graphics, all implemented in the WINGX [52] system of programs. Full-matrix least-squares refinement was carried out by minimizing ( $F_o^2 - F_c^2$ ). All nonhydrogen atoms were refined anisotropically. Hydrogen atoms in all crystal structures attached to carbon atoms in methyl, methylene and methine groups were placed in geometrically idealized positions and refined as riding on their parent atoms where C-H(CH<sub>3</sub>) = 0.96 Å with U<sub>iso</sub> (H) = 1.5 U<sub>eq</sub>(C), C-H(CH<sub>2</sub>) = 0.97 Å with U<sub>iso</sub> (H) = 1.2 U<sub>eq</sub>(C) and

**Table 1**  
The crystal data and refinement parameters for **1**, **2**, **3**, **4** and **6**.

Compound	1	2	3	4	6
<b>Crystal data</b>					
Chemical formula	C <sub>9</sub> H <sub>12</sub> N <sub>4</sub> S	C <sub>10</sub> H <sub>15</sub> N <sub>5</sub> S	C <sub>9</sub> H <sub>12</sub> N <sub>4</sub> OS	C <sub>19</sub> H <sub>26</sub> Cl <sub>2</sub> N <sub>4</sub> ORuS	C <sub>19</sub> H <sub>26</sub> Cl <sub>2</sub> N <sub>4</sub> ORuS
<i>M<sub>r</sub></i>	208.29	237.33	232.29	532.48	530.47
Cell setting, space group	Monoclinic, <i>P</i> 2 <sub>1</sub> / <i>n</i>	Monoclinic, <i>P</i> 2 <sub>1</sub> / <i>n</i>	Triclinic, <i>P</i> 1	Triclinic, <i>P</i> 1	Monoclinic, <i>P</i> 2 <sub>1</sub> / <i>n</i>
<i>a</i>	5.0296(5), 10.7663(5), 19.2282(13)	10.2794(9), 5.0985(4), 22.9490(18)	5.0070(3), 10.2188(6), 11.5523(8)	8.498(5), 10.123(5), 14.094(5)	12.5788(3), 10.1246(2), 17.3679(4)
<i>b</i>					
<i>c</i> (Å)					
$\alpha$	90	90	67.480(6)	102.726(5)	90
$\beta$	93.837(6)	96.137(8)	83.249(5)	94.308(5)	90.126(2)
$\gamma$ (°)	90	90	77.024 (5)	102.265 (5)	90
<i>V</i> (Å <sup>3</sup> )	1038.88 (13)	1195.9 (13)	531.74 (6)	1146.2 (10)	2211.89 (9)
<i>Z</i>	4	4	2	2	4
No. of reflections for cell measurement	926	1476	2406	4253	4630
$\theta$ range (°) for cell measurement	3.7–28.6	3.6–28.1	4.1–28.9	3.6–28.3	3.8–28.5
$\mu$ (mm <sup>−1</sup> )	0.28	0.25	0.28	1.02	1.06
Crystal form, colour	Prism, Orange	Prism, Orange	Prism, Colourless	Prism, Red	Prism, Red
Crystal size (mm)	0.42 × 0.21 × 0.18	0.52 × 0.33 × 0.24	0.58 × 0.33 × 0.27	0.36 × 0.28 × 0.12	0.27 × 0.06 × 0.05
<b>Data collection</b>					
Absorption correction	Multi-scan	Multi-scan	Multi-scan	Gaussian	Analytical
<i>T<sub>min</sub></i> , <i>T<sub>max</sub></i>	0.979, 1.000	0.978, 1.000	0.993, 1.000	0.788, 0.915	0.804, 0.950
No. of measured, independent and observed [ <i>I</i> > 2σ ( <i>I</i> )] reflections	3684, 1818, 1373	3980, 2095, 1828	7801, 2531, 2082	7613, 4007, 3528	9974, 3875, 3192
<i>R<sub>int</sub></i>	0.023	0.018	0.024	0.020	0.035
$\theta$ values (°)	$\theta_{\max}$ = 25.0, $\theta_{\min}$ = 2.8	$\theta_{\max}$ = 25.0, $\theta_{\min}$ = 3.2	$\theta_{\max}$ = 29.3, $\theta_{\min}$ = 3.4	$\theta_{\max}$ = 25.0, $\theta_{\min}$ = 3.0	$\theta_{\max}$ = 25.0, $\theta_{\min}$ = 3.5
Range of <i>h</i> , <i>k</i> , <i>l</i>	<i>h</i> = −5 → 5, <i>k</i> = −9 → 12, <i>l</i> = −22 → 12	<i>h</i> = −8 → 12, <i>k</i> = −5 → 6, <i>l</i> = −27 → 23	<i>h</i> = −6 → 6, <i>k</i> = −13 → 13, <i>l</i> = −15 → 15	<i>h</i> = −10 → 9, <i>k</i> = −12 → 11, <i>l</i> = −14 → 16	<i>h</i> = −14 → 14, <i>k</i> = −12 → 12, <i>l</i> = −18 → 20
<b>Refinement</b>					
<i>R</i> [ <i>F</i> <sup>2</sup> > 2σ ( <i>F</i> <sup>2</sup> )], <i>wR</i> [ <i>F</i> <sup>2</sup> ], <i>S</i>	0.060, 0.158, 1.08	0.041, 0.100, 1.08	0.038, 0.098, 1.06	0.034, 0.075, 1.09	0.034, 0.080, 1.03
No. of reflections	1818	2095	2531	4740	3875
No. of parameters	132	151	141	372	288
No. of restraints	0	0	0	4	0
H-atom treatment	Treated by a mixture of independent and constrained refinement	Treated by a mixture of independent and constrained refinement	Treated by a mixture of independent and constrained refinement	Treated by a mixture of independent and constrained refinement	Treated by a mixture of independent and constrained refinement
Weighting scheme	$w = 1/[\sigma^2(F_o^2) + (0.0746P)^2]$	$w = 1/[\sigma^2(F_o^2) + (0.0441P)^2]$	$w = 1/[\sigma^2(F_o^2) + (0.045P)^2]$	$w = 1/[\sigma^2(F_o^2) + (0.0273P)^2]$	$w = 1/[\sigma^2(F_o^2) + (0.0329P)^2]$
$\Delta\rho_{\max}$ $\Delta\rho_{\min}$ (e Å <sup>−3</sup> )	0.3616[P] where <i>P</i> = ( <i>F<sub>o</sub></i> <sup>2</sup> + 2 <i>F<sub>c</sub></i> <sup>2</sup> )/3 0.26, −0.25	0.2918[P] where <i>P</i> = ( <i>F<sub>o</sub></i> <sup>2</sup> + 2 <i>F<sub>c</sub></i> <sup>2</sup> )/3 0.17, −0.17	0.0866[P] where <i>P</i> = ( <i>F<sub>o</sub></i> <sup>2</sup> + 2 <i>F<sub>c</sub></i> <sup>2</sup> )/3 0.23, −0.23	0.7279[P] where <i>P</i> = ( <i>F<sub>o</sub></i> <sup>2</sup> + 2 <i>F<sub>c</sub></i> <sup>2</sup> )/3 0.59, −0.64	1.9538[P] where <i>P</i> = ( <i>F<sub>o</sub></i> <sup>2</sup> + 2 <i>F<sub>c</sub></i> <sup>2</sup> )/3 0.73, −0.59



C–H(CH) = 0.98 Å with  $U_{\text{iso}}(\text{H}) = 1.2 U_{\text{eq}}(\text{C})$ . Positions of all other hydrogen atoms were taken from  $\Delta F$  map and refined as riding, while their  $U_{\text{iso}}$  were refined. Atoms C18 form the terminal methyl group form  $\eta^6$ -*p*-cymene in complex **6** showed large displacement parameters. The electron-density difference map revealed alternate sites for this C atom, therefore, an effort to model the disorder was made. Atom C18 was found to be disordered over two sites A and B with site occupancy factors of 0.60 (5) and 0.40 (5), respectively. After the refinement, atom C18B was still found to be disordered, but the electron-density difference map did not reveal alternate sites for C18B, and non-Fourier peak in the region exceeds  $0.3 \text{ e Å}^{-3}$ . Crystal data and experimental details of the structures determination for ligands **1**, **2** and **3** and corresponding complexes **4** and **6** are listed in Table 1.

## 2.4. Solution studies

### 2.4.1. HSA-binding experiments

The protein binding study was performed by tryptophan fluorescence quenching experiments using HSA ( $2.0 \times 10^{-6} \text{ M}$ ) in a buffer (10 mM Tris–HCl and 150 mM NaCl at pH 7.4). Fluorescence spectra were recorded from 300 to 450 nm at an excitation wavelength of 295 nm. The fluorescence spectra of the ligands and complexes in buffer solutions were recorded under the same experimental conditions. The fluorescence quenching is described by the Stern–Volmer relation (Eq. (3)) (see ESI), similarly as described below for CT-DNA binding studies.

The values of  $K$  and  $n$  were obtained from the intercept and slope of the plots of  $\log(F_0 - F)/F$  versus  $\log[Q]$  using Eq. (1) (see ESI).

Kinetics and mechanism of the interaction between complex **4** and HSA were studied by conventional UV–Vis spectrophotometry recording the change of the absorbance (in the range between 300 and 800 nm) with the time (Fig. S11, ESI). The reaction was initiated by mixing the solutions in quartz cuvette and followed at three different temperatures (288, 298 and 308 K) several hours. According to the observed kinetic traces, second-order rate constants and thermodynamic parameters ( $\Delta H^\circ$  and  $\Delta S^\circ$ ) were calculated using Microsoft Excel 2007 and Origin Pro 8.

### 2.4.2. DNA-binding studies

Interactions of ligands **1–3** and complexes **4–6** with CT-DNA have been studied with UV spectroscopy in order to investigate the possible binding modes to CT-DNA and to calculate the binding constants to CT-DNA,  $K_b$ . The binding constants,  $K_b$ , of the compounds with CT-DNA have been determined using the UV spectra of the compound recorded for a constant concentration ( $8.0 \times 10^{-5} \text{ M}$ ) in the absence or presence of CT-DNA for diverse  $r$  (0 to 2.2) values. From the absorption data, the binding constant  $K_b$  was determined from a plot of  $[\text{DNA}]/(\epsilon_a - \epsilon_f)$  vs.  $[\text{DNA}]$  using Eq. (2) (see ESI).

The competitive binding of each compound against EB (3,8-Diamino-5-ethyl-6-phenylphenanthridinium bromide) has been investigated with fluorescence spectroscopy in order to establish whether the compound can displace EB from its CT-DNA–EB complex. The CT-DNA–EB complex was prepared by adding  $1.8 \times 10^{-4} \text{ M}$  CT-DNA and  $1.2 \times 10^{-4} \text{ M}$  EB in a buffer (10 mM Tris–HCl and 150 mM NaCl at pH 7.4). Recording of fluorescence spectra was carried out using RF-1501 PC spectrofluorometer by keeping the concentration of CT-DNA–EB complex constant while varying the compound concentration from 0 to  $2.0 \times 10^{-4} \text{ M}$ . The fluorescence emission spectra were measured in the wavelength range of 550–700 nm with an excitation wavelength at 520 nm.

The Stern–Volmer constant  $K_{\text{SV}}$  is used to evaluate the quenching efficiency for each complex according to Eq. (3) [53,54] (see ESI).  $K_{\text{SV}}$  is the Stern–Volmer constant and can be obtained by the slope of the diagram  $F_0/F$  versus  $[Q]$ .

## 2.5. Computational chemistry

### 2.5.1. Quantum mechanics and molecular docking

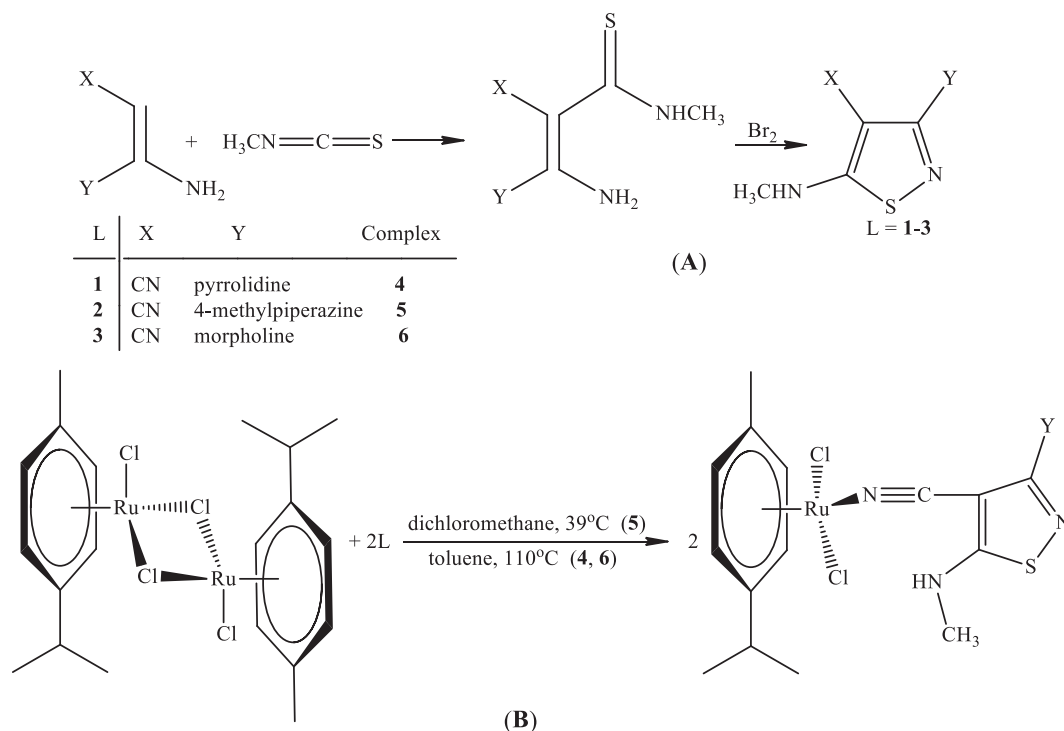
Geometry optimizations were carried out with Gaussian 09 D.01 program [55], using hybrid functional of Truhlar and Zhao (M06) [56] and in each case, the SDDall basis set was used [57]. Starting geometries were taken either from experimental X-ray structures or were modeled, starting with conformational search from which the best hits were taken in order to pre-optimize them using the semi-empirical methods (MOPAC2016 [58]/PM6-D3H4 [59] Hamiltonian). The systems were treated within restricted formalism. All calculations were performed with toluene (ligands) or H<sub>2</sub>O (complexes) as solvent by use of the Integral Equation Formalism Polarizable Continuum Model (IEFPCM) as implemented in Gaussian 09. Geometry optimizations were conducted without symmetry constraints. The minimum energy was achieved in all cases which were confirmed by the frequency calculations for each optimized structure. The best conformations along with atom charges have been taken for molecular docking simulations.

**2.5.1.1. Docking.** Molecular docking of ligands and corresponding ruthenium(II) complexes was simulated to either three-dimensional X-ray structure of human serum albumin (HSA), PDB (Protein Data Bank) code 1HK1 [60] and 1O9X [61] or to the double-stranded (ds) dodecamer sequence of 5'-d(CCTCTG\*GTCTCC)-3'\*5'-d(GGAGACCAGAGG)-3' the three-dimensional X-ray structures of Lippard's DNA duplex (PDB code 1AIO) [62]. Docking processes were carried out using AutoDock 4.2.6 [63] and AutoDock Vina [64] software equipped with the graphical user interface (GUI) AutoDockTools (ADT 1.5.6rc3) [63]. Adapted GOLD [65] suite of programs (Hermes and Gold), 5.6.2 release [66] were used for docking as well.

Details of Autodock 4.2.6 docking procedures are described elsewhere [39,67]. Since ruthenium is not included in the AutoDock parameter file, extended parameter file including Ru(II) parameters was used [68]. Docking assessment against AutoDock has been validated across two X-ray structures: PDB codes 1HK1 and 1O9X as described in our recent paper [39].

All GOLD calculations were performed with the GoldScore (GS) scoring function. All modifications to the GOLD force-field were made according to Sciortino et al. [66]. The GS parameter file was modified to include parameters of atom types not included in GOLD's database, such as metals and possible coordinating atom groups and, in particular,  $\text{sp}^2$  oxygens (e.g., those of carboxylate group),  $\text{sp}^3$  oxygen of water, and  $\text{sp}^3$  negatively charged oxygens of deprotonated serine, threonine, and tyrosine residues. The metal atom type (M.Ru) was built with the values reported in the literature, the keto (O.pl3), the water oxygen atoms (O.H<sub>2</sub>O) and the  $\text{sp}^3$  negatively charged oxygens were fixed considering the geometry of the electron pairs derived from the valence shell electron pair repulsion (VSEPR) theory. Genetic algorithm (GA) parameters were set with a number of GA runs equal to 50 and a minimum of 100,000 operations. The rest of the parameters, including pressure, a number of islands, niche size, crossover, mutation, and migration were left to default. Docking assessment against GOLD in the case of protein has been already validated by Sciortino et al. [66]. Since modified GOLD forcefield has not been validated against DNA by the authors [66] we carried out a small portion of this process. For this purpose, we took the DNA part of nucleosome structure (PDB code 4KGC [9]) and one of the ruthenium(II) complex RAED-C coordinated to DNA. The results are more or less promising (Fig. S12, ESI) with a best docked conformation close to X-ray one.

HSA molecule was cleaned up from the water and co-crystallized ligands; hydrogens were added and Gasteiger charges were computed. All the ligands used for the docking process were taken from either their X-ray structures or mother macromolecules and optimized by QM using the procedure given above. Finally, the “.mol2” 3D ligand files were extracted from Gaussian outputs along with corresponding charges that



**Scheme 1.** Synthetic route for isothiazole ligands **1**, **2** and **3** (A) and corresponding ruthenium(II)  $[\text{Ru}(\eta^6\text{-}p\text{-cymene})\text{Cl}_2(\text{L})]$  complexes **4**, **5** and **6** (B).

have been used for the docking purpose. The receptor-ligand interactions were calculated and visualized by Discovery Studio Visualizer v17.2.0.16349 [69]. For the DNA docking of the standard  $[\text{Ru}(\text{Ar})(\text{L})(\text{H}_2\text{O})_n]^{2+}$  ( $n = 0, 1, 2$ ) complexes the grid box of  $60 \times 60 \times 60$  points (default spacing is  $0.375 \text{ \AA}$ ) has been used with DG6(N7) atoms taken as its center.

The best GOLD hit (DNA-Ligand) was further optimized by MOPAC-MOZYME PM6 [58] method. This includes preoptimization of hydrogen atoms only with MOPAC's keywords NOOPT and OPT-H following by the full optimization of the whole system using MOZYME. Covalently bounded sphere around ruthenium(II) ion has been further optimized by QM using the above given details.

## 2.6. Biological tests

### 2.6.1. Cell lines

The cell lines used in the study were: MCF-7 (ATCC HTB 22 - human breast adenocarcinoma ER+), HeLa (ATCC CCL 2 - cervix epithelial carcinoma), HT-29 (ATCC HTB 38 - human colon adenocarcinoma), A-549 (ATCC CCL185 - lung carcinoma) and MRC-5 (ATCC CCL 171 - normal fetal lung fibroblasts). The cells were grown in Dulbecco's modified Eagle's medium (DMEM) with 4.5% of glucose, supplemented with 10% of fetal calf serum (FCS, Sigma) and antibiotics and antimycotics solution (Sigma). The cell lines were cultured in flasks (Costar,  $25\text{cm}^2$ ) at  $37^\circ\text{C}$  in the atmosphere of 100% humidity and 5% of  $\text{CO}_2$  (Heraeus). Exponentially growing viable cells were used throughout the assays.

### 2.6.2. Tested substances

Cisplatin and tested compounds were used at concentrations from  $10^{-4} \text{ M}$  to  $10^{-8} \text{ M}$  in order to define  $\text{IC}_{50}$  concentration for a particular time point. The substances were added in a volume of  $10 \mu\text{L well}^{-1}$ .

### 2.6.3. MTT (3-(4,5-dimethyl-2-thiazolyl)-2,5-diphenyl-2H-tetrazolium bromide) assay

Antiproliferative activity was investigated by tetrazolium colorimetric MTT assay [70], as previously described [39]. The effect of the

compounds was expressed as the  $\text{IC}_{50}$  value.

### 2.6.4. Flow cytometry

**2.6.4.1. Cell cycle analysis.** HeLa cells were treated with tested compounds for 48 h at their  $\text{IC}_{50}$  concentrations. After treatment, HeLa cells were washed in cold phosphate buffer (PBS) and incubated for 30 min in 70% ethanol on ice, centrifuged and incubated with 500 mL RNase A ( $100 \text{ units mL}^{-1}$ ) and 500 mL propidium iodide ( $400 \mu\text{g mL}^{-1}$ ) for 30 min at  $37^\circ\text{C}$ . The cell cycle was analyzed by FACS Calibur E440 (Becton Dickinson) flow cytometer and the Cell Quest software. Results were presented as the percentage of cell cycle phases.

**2.6.4.2. Annexin-V-FLUOS assay.** Apoptosis of HeLa cells was evaluated with an Annexin V-FITC detection kit. Treated cells from each sample were collected ( $800 \text{ rpm } 5 \text{ min}^{-1}$ , Megafuge 1.0R, Heraeus, Thermo Fisher Scientific) and the pellet was re-suspended in 1 mL of PBS pH 7.2. HeLa cells were washed twice with cold PBS and then re-suspended in the binding buffer to reach the concentration of  $1 \times 10^6 \text{ cells mL}^{-1}$ . The cell suspension (100 mL) was transferred to 5 mL culture tubes and mixed with Annexin-V (5 mL) and propidium iodide (5 mL). The cells were gently vortexed and incubated for 15 min at  $25^\circ\text{C}$ . After incubation, 400 mL of binding buffer was added to each tube and suspension was analyzed after 1 h on FACS Calibur E440 (Becton Dickinson) flow cytometer. Results were presented as a percent of Annexin-V positive gated cells. The percentage of specific apoptosis was calculated according to Bender et al. [71].

## 3. Results and discussion

The 3,5 diaminoisothiazole derivatives **1–3** were prepared in excellent yields by following a literature protocol [42,43]. These ligands were used for synthesis with the  $[\text{Ru}(\eta^6\text{-}p\text{-cymene})\text{Cl}_2]_2$  in the presence of toluene (complexes **4** and **6**) or dichloromethane (complex **5**) under reflux. All synthesized complexes of the general formula  $[\text{Ru}(\eta^6\text{-}p\text{-cymene})\text{Cl}_2(\text{L})]$  were obtained in good yields (Scheme 1).

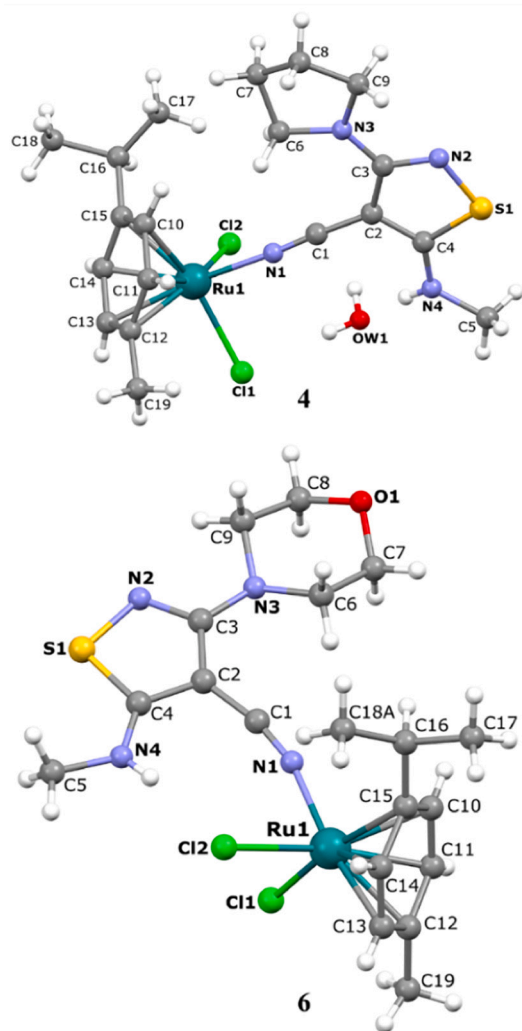


Fig. 2. MERCURY [51] drawings of the molecular structure of complexes 4 and 6 with labeled non-H atoms.

### 3.1. Stability

The detailed syntheses of  $[\text{Ru}(\eta^6\text{-}p\text{-cymene})\text{LCl}_2]$  are presented in Scheme 1. Before use in the biological experiments, the purities of the investigated compounds were determined by UV–Vis and NMR methods (Figs. S13 and S14, ESI). Because of the probable metalation of S atoms in DMSO with Ru metal, we first tested the chemical stability of  $N$ -coordinated  $[\text{Ru}(\eta^6\text{-}p\text{-cymene})\text{LCl}_2]$  in 1% DMSO (MTT assay) through the above methods. As shown in Fig. S13 (ESI), the shape of peaks and their relative position remained unchanged during all tested time points (24 h). Taken together, these data indicated that the structures of  $[\text{Ru}(\eta^6\text{-}p\text{-cymene})\text{LCl}_2]$  are stable in DMSO solution at least for 48 h.

### 3.2. Spectroscopic analysis

The FT-IR,  $^1\text{H}$  NMR,  $^{13}\text{C}\{^1\text{H}\}$  NMR, and UV–Vis were used to characterize the synthesized compounds (Figs. S1–S10, ESI). The spectral data obtained were in good agreement with the proposed structures.

Perhaps the most important analyses use FT-IR results. The IR spectra of the complexes displayed a strong band in the region of  $2200\text{--}2239\text{ cm}^{-1}$  which is characteristic of the  $\text{-C}\equiv\text{N}$  functional group. This band is located at a higher frequency relative to the same band in the spectra of the uncoordinated ligands (Fig. S3, ESI). It is

obvious that the ligands are coordinated to the Ru(II)-ion via the  $\text{-C}\equiv\text{N}$  group. The complexes also displayed  $\nu = \text{CH}$ ,  $\nu_{\text{CH}}$ , and  $\nu_{\text{C}=\text{C}}$  absorptions in the region of  $3266\text{--}3432\text{ cm}^{-1}$ ,  $2923\text{--}2969\text{ cm}^{-1}$  and  $1524\text{--}1580\text{ cm}^{-1}$ , respectively.

UV–Vis spectra for all complexes were recorded from 200 to 800 nm in methanol. Absorption bands that were observed in the region  $337\text{--}342\text{ nm}$  region can be attributed to  $n\text{-}\pi^*$  and  $\pi\text{-}\pi^*$  ligand-centered transitions, respectively. Furthermore, the low-intensity bands in the visible region  $390\text{--}430\text{ nm}$  could be assigned to the metal to ligand ( $d\pi\text{-}\pi^*$ ) charge transfer (MLCT) transition from the filled 4d orbital to the empty  $\pi^*$  orbital, similar to the MLCT observed in other reported Ru(II)-arene complexes [72].

The NMR spectra were recorded in  $\text{CDCl}_3$  to confirm the bonding of the ligand to the ruthenium(II) ion. In the  $^1\text{H}$  NMR spectra from each complex, a sharp singlet appeared at around 2.19–2.99 ppm that has been assigned to the  $\text{CH}_3$  group. The complexes 5 and 6 show two triplets each originating from protons belonging to 4-methylpiperazine ( $\delta = 2.51\text{ ppm}$  and  $\delta = 3.58\text{ ppm}$ ) and morpholine ( $\delta = 3.50\text{ ppm}$  and  $\delta = 3.78\text{ ppm}$ ). Complex 4 is the only one to show quintet at  $\delta = 1.95$ , which is derived from pyrrolidine protons. In complex 5, an additional methyl signal is observed at 2.33 ppm, which is due to the methyl group in the 4-methylpiperazine. All the other signals belong to ruthenium- $p$ -cymene.

### 3.3. Crystal structures

The molecular structures of 1, 2 and 3 are presented in Fig. S15 (see ESI) while the selected bond lengths and bond angles are presented in Table S1 (see ESI). Both, 1 and 2, structures crystallize in centrosymmetric  $P2_1/n$  while 3 crystallizes in the triclinic crystal system and  $P\bar{1}$  space group, and all asymmetric parts of the unit cells in the crystal structures contains neutral molecules. If we validate the conformation of ligand structures through the values of dihedral angles (Table S1, ESI) we can notice that the isothiazole-4-carbonitrile part in all three compounds (1, 2, 3) can be considered as almost perfectly planar. On the other hand, pyrrolidine, methylpiperazine and morpholine part in 1, 2 and 3, respectively, gives rise to conformational differences since the methylpiperazine in 2 and morpholine in 3 are adopting the same chair conformation where the puckering parameters are:  $Q_T = 0.556(2)\text{ \AA}$ ,  $\theta_2 = 177.3(2)^\circ$  and  $Q_T = 0.552(2)\text{ \AA}$ ,  $\theta_2 = 174.3(2)^\circ$ , respectively, while the five-membered pyrrolidine in 1 has almost planar conformation with puckering parameters  $q_2 = 0.118(5)\text{ \AA}$ ,  $\varphi_2 = -84(2)^\circ$ . The planarity and conformation differences of 1, 2 and 3 compounds are visually depicted in Fig. S15 (see ESI) which displays an overlay of three structures. The structures of all three ligands are stabilized by two hydrogen bonds between the cyano group of one molecule and the amino group of another molecule, as follows: 2.327 (1), 2.232 (2), 2.242 (3).

A perspective view of the molecular structures of complexes 4 and 6 with the adopted atom-numbering scheme is shown in Fig. 2. Selected metal-ligand bond lengths, bond angles, and torsion angles are listed in Table 2. Complex 4 crystallizes in the triclinic crystal system and  $P\bar{1}$  space group where each asymmetric unit consists of two moieties: one neutral Ru- $p$ -cymene-complex and one water molecule. In the crystal structure of 4 the Ru(II) ion is coordinated by two  $\text{Cl}^-$  ions and nitrogen donor atom of 1 with the  $\text{Ru1-N1}$  bond distance of  $2.064(3)\text{ \AA}$ , while  $\text{Ru1-}Ar_{\text{centroid}}$  bond distance ( $\pi$  bond) has the value of  $1.661\text{ \AA}$ . The crystal packing of complex 4 is arranged by hydrogen bonds involving  $\text{H}_2\text{O}$  molecules and nitrogen and chlorine atoms (Table S2, ESI).

Complex 6 crystallizes in the monoclinic crystal system and  $P2_1/n$  space group where each asymmetric unit consists of the one neutral form of Ru- $p$ -cymene-complex. In the crystal structure of 6, the Ru(II) ion is coordinated by two  $\text{Cl}^-$  ions and nitrogen donor atom of ligand 3 with a  $\text{Ru1-N1}$  bond distance of  $2.059(3)\text{ \AA}$ .  $\text{Ru1-}Ar_{\text{centroid}}$  bond distance ( $\pi$  bond) in 6 has a value of  $1.662\text{ \AA}$ . The crystal packings of all ligands 1, 2 and 3 are arranged in forms of dimers that are formed by N-

**Table 2**  
Selected geometric parameters for complexes **4** and **6**.

	<b>4</b>	<b>6</b>
Bond length [Å]		
Ru1—N1	2.064 (3)	2.059 (3)
Ru1—Cl1	2.412 (1)	2.395 (1)
Ru1—Cl2	2.423 (2)	2.422 (1)
Ru1—C10	2.158 (4)	2.154 (4)
Ru1—C11	2.183 (4)	2.166 (4)
Ru1—C12	2.210 (4)	2.218 (3)
Ru1—C13	2.160 (4)	2.175 (3)
Ru1—C14	2.154 (4)	2.147 (4)
Ru1—C15	2.190 (4)	2.194 (3)
Bond angles [°]		
Cl1—Ru1—Cl2	88.36 (4)	86.91 (6)
N1—Ru1—Cl1	86.61 (8)	83.40 (9)
N1—Ru1—Cl2	84.14 (8)	81.97 (8)
N1—Ru1—C10	92.37 (1)	91.91 (1)
N1—Ru1—C11	94.92 (1)	110.92 (1)
N1—Ru1—C12	121.28 (1)	145.91 (1)
N1—Ru1—C13	159.73 (2)	168.58 (1)
N1—Ru1—C14	153.3 (2)	131.17 (1)
N1—Ru1—C15	115.71 (2)	100.03 (1)
Torsion angles [°]		
Ru1—C15—C16—C17	−68.4 (6)	−177.6 (3)
Ru1—C15—C10—C11	−54.1 (3)	−54.5 (3)
Ru1—C11—C12—C13	−53.1 (3)	−52.1 (3)
Ru1—C13—C12—C19	−123.6 (4)	−123.9 (4)
Ru1—C13—C14—C15	−53.9 (4)	−55.4 (3)

H··N hydrogen bonds; the crystal structure of **6** is stabilized by intramolecular hydrogen bond involving NH group of ligand **3** and Cl<sup>−</sup> ion (Table S2, ESI).

### 3.4. Interaction of the ligands and complexes with HSA

The most important role of the serum albumins is the transportation of many biologically active compounds (drugs, natural products, metal ions, metal complexes, etc.) in the blood. The investigation of binding interactions between the biologically potent compounds and HSA can be important in exploring their potential biological activity and application. The degree of binding of the compound to albumin determines the availability of the compound in the organism. It is well known that only the unbound fraction of the compound (drug) in plasma is free to cross the cell membrane and to produce pharmacological effects [73]. In order to investigate the structural changes in HSA caused by the addition of ligand or complex and determine the binding constant (*K*) and the number of binding sites (*n*) for the complex formed between ligand or complex and HSA, absorption and fluorescence spectra were measured.

The study of ligand binding to a variety of (usually biological) molecules is often performed using fluorescence quenching methodology. Quenching is any process that decreases the fluorescence intensity (excited-state reactions, molecular rearrangements, energy transfer, ground-state complex formation, and collisional quenching). The quenching mechanism is usually classified as either dynamic or static quenching. HSA solutions exhibit a strong fluorescence emission with a peak at about 350 nm, due to the tryptophan residues, when excited at 295 nm [54]. The fluorescence spectra of HSA with different concentrations of ligands (**1–3**) and complexes (**4–6**) were recorded and are shown in Figs. S16–S21 (ESI).

As shown in Figs. S16–S21 (ESI), adding of complex to the HSA solution, the fluorescence intensity of HSA decreased gradually with an increase in complex concentration. This result suggests that complex can interact with HSA and quench its intrinsic fluorescence. The addition of ligands (**1–3**) or their complexes (**4–6**) to HSA results in fluorescence quenching (up to about 15–20% of the initial fluorescence intensity of HSA for ligands and about 30–70% for complexes) (Fig. 3).

The *K*<sub>SV</sub> and quenching constants (*k*<sub>q</sub>) of the interactions of the compounds with the albumins were calculated (Table 3) from the corresponding Stern-Volmer plot (see inset in Figs. S16–S21, ESI) and Stern-Volmer quenching equation (Eq. (3)) (see ESI), where the fluorescence lifetime of tryptophan in HSA was taken as  $\tau_0 = 10^{-8}$  s.

As seen in Table 3, the quenching constants ( $> 10^{11} \text{ M}^{-1} \text{ s}^{-1}$ ) are higher than diverse kinds of quenchers for biopolymers fluorescence ( $10^{10} \text{ M}^{-1} \text{ s}^{-1}$ ), suggesting that the interaction of the ligands and complexes with the albumins takes place via a static quenching mechanism, which indicates the formation of a new conjugate between each complex and HSA [67]. Using the equation (Eq. (3)) (see ESI), the values of *K* (association binding constant) and *n* (number of binding sites per albumin) for the ligands **1–3** and complexes **4–6** were obtained from the intercept and slope of the plots of  $\log(F_0 - F)/F$  versus  $\log [Q]$  (Figs. S22 and S23, ESI).

The values of the binding constant, *K* and those of *n* are given in Table 3. The calculated value of *n* is around one for all of the compounds, indicating the existence of just a single binding site in HSA for all of the compounds. From the values of *K*, it is inferred that complex **4** interacts with HSA more strongly than the rest of the compounds. The HSA-binding constants of complexes **4** ( $1.04 \times 10^6 \text{ M}^{-1}$ ), **5** ( $2.80 \times 10^5 \text{ M}^{-1}$ ) and **6** ( $4.60 \times 10^5 \text{ M}^{-1}$ ) showed that there is a strong binding force between complex and HSA, which implies that HSA can transfer investigated complexes toward potential biotargets. As shown in Table 3, ligands have lower binding affinity for albumin in relation to their complexes.

UV–Vis absorption measurement is a very simple but effective method that is used to investigate structural changes and to explore complex formation. The changes (hypochromism/hyperchromism and/or red shift/blue shift) observed in the UV spectra during titration may provide evidence of the existing interaction mode of compounds and HSA. Collisional (dynamic) quenching only affects the excited states of the fluorophores and, thus, no changes in the absorption spectra are expected. In contrast, the groundstate complex formation will frequently result in perturbation of the absorption spectrum of the fluorophore [52]. In the present study, the change in the UV–Vis absorption spectra of the HSA-compound system (Fig. 4 and Figs. S24–S28, ESI) was measured under simulated physiological conditions.

HSA has a weak absorption peak at about 280 nm because of the cumulative absorption of three aromatic amino acid residues (Trp, Tyr, and Phe). The absorption intensity at 280 nm increased progressively (Fig. 4 and Figs. S24–S28, ESI) with the addition of ligands **1–3** or complexes **4–6**, suggesting that the complex was formed between ligand or complex and HSA and that the polypeptide chain of HSA successively unfolded upon the addition of this complex. The maximum peak position of HSA-compounds was shifted slightly toward the lower wavelength region. The change in  $\lambda_{\text{max}}$  indicates the change in polarity around the tryptophan residue and the change in the peptide strand of HSA molecules and hence the change in hydrophobicity [74]. This result reconfirms that the probable fluorescence quenching mechanism of HSA by compounds is a static quenching process [75].

#### 3.4.1. Kinetics

Metal complexes can bind to HSA by different binding modes. Associative manner includes the replacement of labile aqua (or chlorido) ligand by protein donor to the metal center. This binding mechanism is usually governed by the thermodynamic stability and kinetic inertness of the complexes. On the other hand, the dissociative mode is specific for labile complexes that during the interaction decompose partially or completely. Considering the rate constants and activation parameters (Table 4), studied interaction is very slow, while the negative value of the entropy of activation indicates an associative mode that includes strong coordinate (covalent) bonding of the complex through the displacement of the labile aqua (or chlorido) ligand by protein donor atoms preserving its original entity. IR spectral changes confirmed lower affinity binding of this complex, and non-dissociated complex is



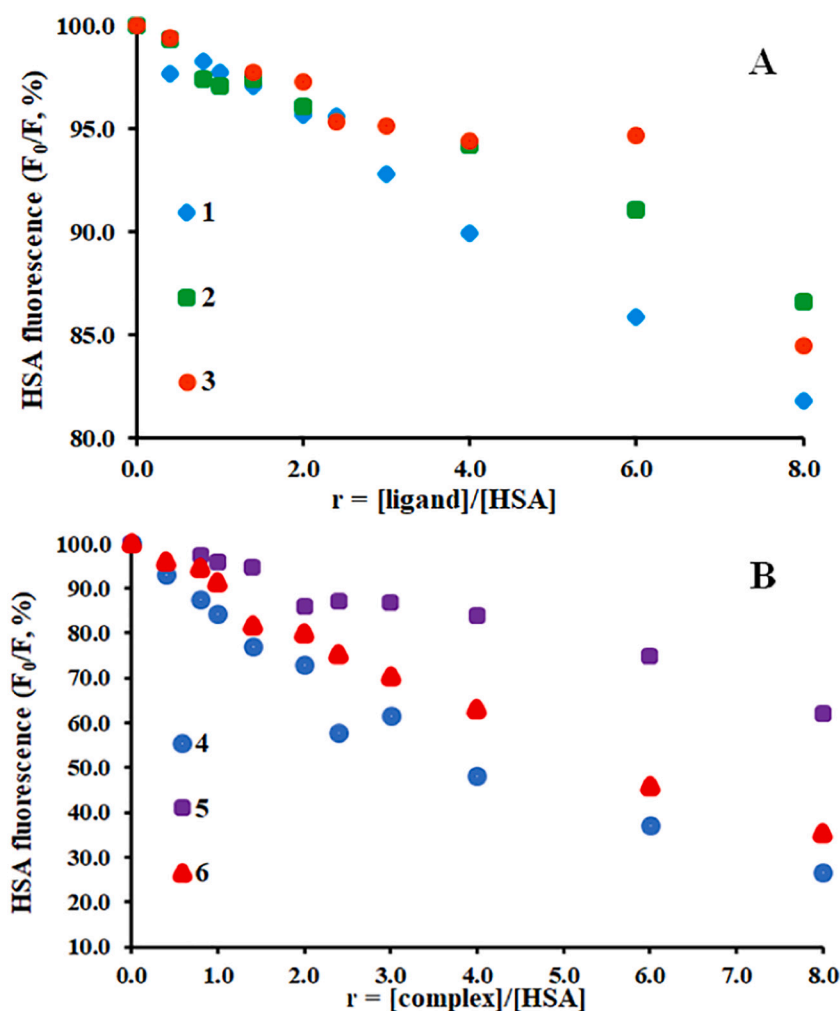


**Fig. 3.** Plot of EB relative fluorescence intensity at  $\lambda_{\text{em}} = 350$  nm (%) versus  $r$  ( $r = [\text{complex}]/[\text{HSA}]$ ) for ligands (A) and their complexes (B) in buffer solution (10 mM Tris-HCl and 150 mM NaCl at pH 7.4).

**Table 3**

The HSA binding constants and parameters ( $K_{\text{SV}}$ ,  $k_q$ ,  $K$ ,  $n$ ) for the ligands 1–3 and complexes 4–6.

Compound	$K_{\text{SV}}$ ( $\text{M}^{-1}$ )	$K_q$ ( $\text{M}^{-1} \text{s}^{-1}$ )	$R^{2a}$	$K$ ( $\text{M}^{-1}$ )	$\Delta G$ (kcal) <sup>b</sup>	$N$	$R^{2a}$
1	$1.45 \times 10^4$	$1.45 \times 10^{12}$	0.985	$4.95 \times 10^4$	−6.40	1.12	0.987
2	$7.17 \times 10^3$	$7.17 \times 10^{11}$	0.963	$7.28 \times 10^3$	−5.27	0.98	0.990
3	$1.20 \times 10^4$	$1.20 \times 10^{12}$	0.988	$4.39 \times 10^4$	−6.33	1.13	0.987
4	$1.47 \times 10^5$	$1.47 \times 10^{13}$	0.974	$1.04 \times 10^6$	−8.21	1.17	0.984
5	$2.93 \times 10^4$	$2.93 \times 10^{12}$	0.985	$2.80 \times 10^5$	−7.43	1.20	0.983
6	$7.71 \times 10^4$	$7.71 \times 10^{12}$	0.985	$4.60 \times 10^5$	−7.72	1.16	0.980

<sup>a</sup>  $R^2$  is the correlation coefficient.

<sup>b</sup>  $\Delta G^\circ = -RT \ln K$ .

assumed to bind mainly on the protein. UV–Vis studies showed minimal spectral changes in the presence of HSA, implying small, or no rearrangement in the coordination sphere of Ru(II) ion. Combining the results of the solution studies applied in this work, we can conclude that the binding of the ligand–complex to HSA is thermodynamically less favored.

X-ray single crystal structures reported for protein–Ru-*p*-cymene complex adducts often show coordination of amino acids His or Glu to the metal center [76–82], and coordination of Lys, Arg, Asp and Cys side chains occur as well [77,82,83]. Coordination of one or two of these side chains is typical, and the loss of *p*-cymene ligand can be detected in some cases as well [76,77,83]. Apo-ferritin coordinated ([NHis, NHis, OGLu]) is the only reported structure, where the

coordination sphere of Ru-*p*-cymene is saturated by the donor groups of the protein only [77]. Metal complexes studied display different binding modes. Our results suggest the following mechanism for albumin binding: as initial step a protein donor atom coordinates monodentately to the metal center replacing the aqua (or chlorido) leaving the group in the metal complex (slow associative binding), that is optionally followed by coordination of additional protein donor atom (s) and consecutive release of the original ligand (dissociative binding). The binding mechanism is governed by the thermodynamic stability and kinetic inertness of the complexes.

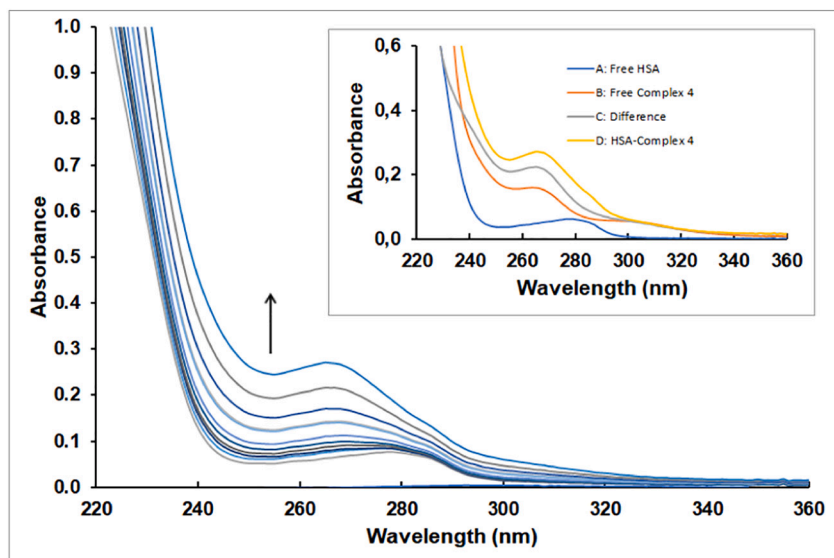


Fig. 4. Absorption spectra of HSA ( $2 \times 10^{-6}$  M), with various amounts of the **4** complex ( $0-1.6 \times 10^{-5}$  M) at room temperature. Inset: UV-Vis absorption spectra of HSA in the absence and presence of complex **4**: A, the absorption spectrum of HSA only; B, the absorption spectrum of complex **4** only; C, the difference between the absorption spectrum of HSA-complex **4** and complex **4**; D, the absorption spectrum of HSA-complex **4**.

Table 4

Second-order rate constants and activation parameters for the reaction between complex **4** and HSA.

T (K)	$k_1$ ( $\text{M}^{-1} \text{s}^{-1}$ )	$\Delta H^\ddagger$ ( $\text{kJ mol}^{-1}$ )	$\Delta S^\ddagger$ ( $\text{JK}^{-1} \text{mol}^{-1}$ )
288	$(6.80 \pm 0.02) \times 10^{-4}$	$53 \pm 2$	$-154 \pm 7$
298	$(1.86 \pm 0.03) \times 10^{-4}$		
308	$(3.07 \pm 0.03) \times 10^{-4}$		

### 3.5. Interaction of the ligands and complexes with CT-DNA

Transition metal complexes can bind to DNA via both covalent and/or noncovalent (intercalation, electrostatic or groove binding) interactions [84,85]. Absorption spectroscopy is one of the most useful methods for studying the binding of compounds to DNA [86]. The interaction of the metal complexes with the base pairs of DNA is usually followed by a hypochromic shift with a small red/blue shift [87]. On the other hand, the hyperchromic shift might be ascribed to external contact (electrostatic interactions) or to the capacity of the complex to uncoil the helix structure of DNA [88,89]. The absorption spectra of the ligand **1** and complex **4** in the absence and presence of CT-DNA are shown in Fig. 5 (others are given in Figs. S29-S32, ESI).

In the presence of CT-DNA, the absorption band of ligand **1** and complex **4** at 264 nm exhibited hyperchromism (as in all other investigated compounds). This increasing absorbance indicates that there are interactions between the complex and the base pairs of DNA. The extent of the hyperchromism in the charge transfer band is generally consistent with the strength of interaction [90]. As DNA double helix possesses many hydrogen bonding sites which are accessible both in the minor and in the major grooves, N and O atoms on ligands likely form hydrogen bonds with DNA, which may contribute to the hyperchromism observed in absorption spectra. The increasing absorbance indicates that there are groove binding modes [91]. The observed hyperchromicity for ligands and complexes after addition of CT-DNA suggested their electrostatic interaction with DNA. Also, ligands containing aromatic moiety in the complex may bind to the base pairs of DNA in intercalative mode [92]. The intrinsic binding constants  $K_b$  of ligands and complexes were calculated according to the classic equation (Eq. (1)) and are given in Table 5. The calculated  $K_b$  values for ligands (**1-3**) and complexes (**4-6**), were obtained from the plot of  $[\text{DNA}]/(\epsilon_a - \epsilon_f)$  vs.  $[\text{DNA}]$  (see Figs. S33 and S34, ESI) (Table 5), suggest a moderate binding of the compounds to CT-DNA.

The  $K_b$  values of complexes **5** and **6** are lower than their ligands **2** and **3** (Table 5) suggesting that complexes have lower binding affinity

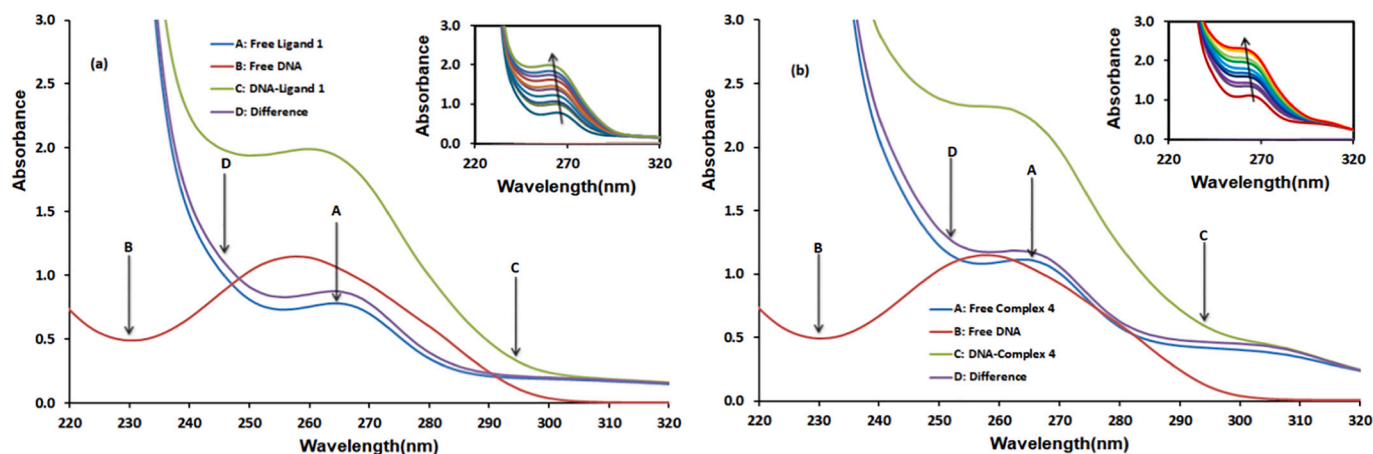


Fig. 5. UV-Vis absorption spectra of (a) ligand **1** and (b) complex **4** in the absence and presence of CT-DNA: A, the absorption spectrum of ligand **1** or complex **4** only; B, the absorption spectrum of DNA only; C, the absorption spectrum of DNA-compound; D, the difference between the absorption spectrum of DNA-compound complex and compound. Inset: absorption spectra of the compound in the presence of a range of DNA concentrations.  $[\text{Ligand}] = [\text{Complex}] = 8.0 \times 10^{-5} \text{ mol dm}^{-3}$ ,  $[\text{DNA}] = 0-1.7 \times 10^{-4} \text{ mol dm}^{-3}$ .

**Table 5**

The DNA binding constants ( $K_b$ ), calculated from UV spectra and the Stern–Volmer constants ( $K_{SV}$ ), and Quenching constant ( $K_q$ ) calculated from fluorometric spectra.

Compounds	In the absence of EB			In the presence of EB		
	$K_b$ ( $M^{-1}$ )	$\Delta G$ (kcal) <sup>b</sup>	$R^{2a}$	$K_{SV}$ ( $M^{-1}$ )	$K_q$ ( $M^{-1}s^{-1}$ )	$R^{2a}$
1	$2.63 \times 10^4$	−6.03	0.991	$5.39 \times 10^3$	$5.39 \times 10^{11}$	0.941
2	$3.67 \times 10^4$	−6.22	0.915	$2.08 \times 10^3$	$2.08 \times 10^{11}$	0.938
3	$9.17 \times 10^4$	−6.77	0.976	$1.80 \times 10^3$	$1.80 \times 10^{11}$	0.996
4	$4.97 \times 10^4$	−6.41	0.965	$1.34 \times 10^3$	$1.34 \times 10^{11}$	0.967
5	$1.85 \times 10^4$	−5.82	0.987	$1.50 \times 10^3$	$1.50 \times 10^{11}$	0.913
6	$1.04 \times 10^4$	−5.48	0.975	$2.32 \times 10^3$	$2.32 \times 10^{11}$	0.992

<sup>a</sup>  $R^2$  is the correlation coefficient.

<sup>b</sup>  $\Delta G^\circ = -RT \ln K$ .

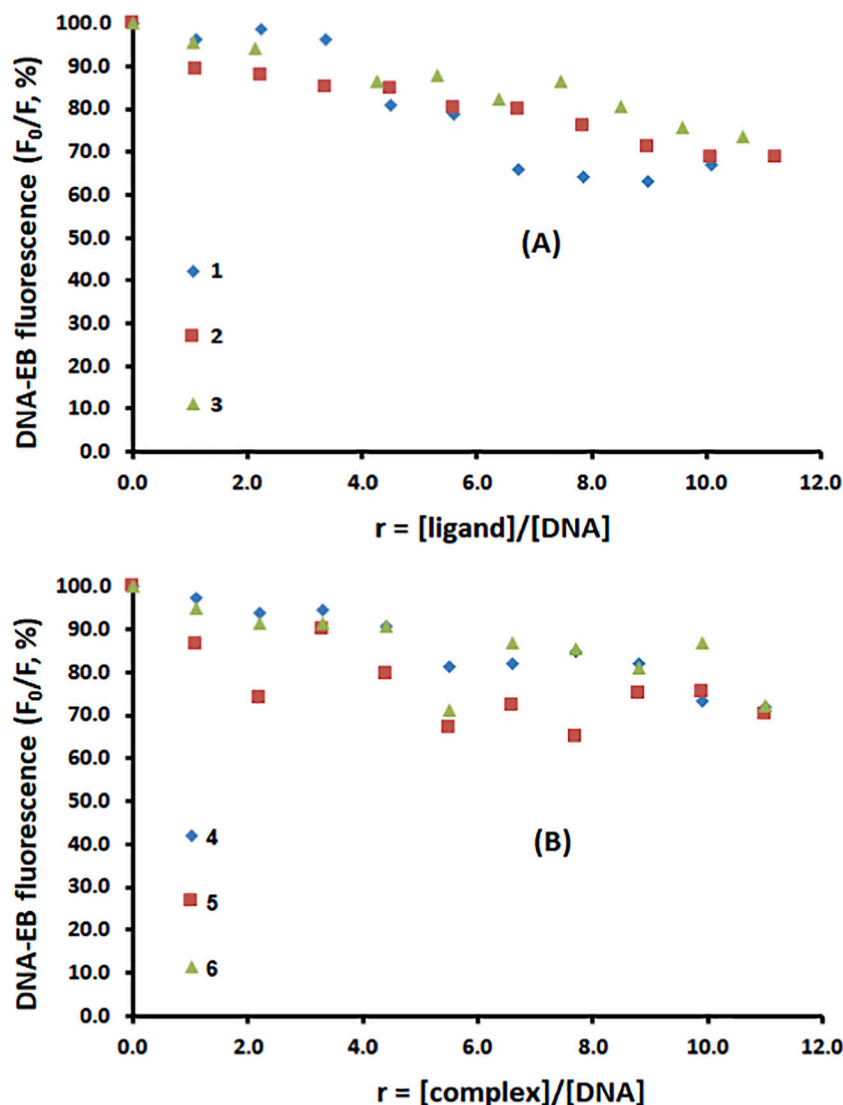


**Fig. 6.** Plot of EB relative fluorescence intensity at  $\lambda_{em} = 613$  nm (%) versus  $r$  ( $r = [\text{complex}]/[\text{DNA}]$ ) for ligands (A) and their complexes (B) in buffer solution (10 mM Tris-HCl and 150 mM NaCl at pH 7.4).

to CT-DNA. On the other hand, complex 4 exhibits higher  $K_b$  value than its ligand. The  $K_b$  values of all compounds are lower than the classical intercalator EB binding affinity for CT-DNA, ( $K_b = 1.23 \times 10^5 M^{-1}$ ) [93] and these values are in agreement with those of well-established groove binding rather than classical intercalation [94].

In order to examine the ability of the compounds to displace EB from the EB-DNA complex, competitive EB binding studies were carried

out with fluorescence measurements. The emission spectra of EB bound to CT-DNA in the absence and presence of ligands or complexes were recorded for  $[\text{DNA}] = 1.8 \times 10^{-4} M$ ,  $[\text{EB}] = 1.2 \times 10^{-4} M$  EB and increasing amounts of each compound. The emission spectra of EB bound to CT-DNA in the presence of a compound 1–6 derived for diverse  $r$  values are shown in Figs. S35–40 (see ESI). The intensity of the emission band of the CT-DNA-EB complex at 613 nm decreased with

**Table 6**  
X-Ray vs. DFT bond length for complexes **4** and **6**.<sup>a</sup>

X-ray		DFT	
Complex 4			
Ru1—N1	2.064 (3)	Ru1—N25	2.0252 (1)
Ru1—C10	2.158 (4)	Ru1—C5	2.2246 (1)
Ru1—C11	2.183 (4)	Ru1—C21	2.1932 (1)
Ru1—C12	2.210 (4)	Ru1—C6	2.2283 (1)
Ru1—C13	2.160 (4)	Ru1—C42	2.2618 (1)
Ru1—C14	2.154 (4)	Ru1—C29	2.2324 (1)
Ru1—C15	2.190 (4)	Ru1—C43	2.2163 (1)
Ru1—Cl1	2.412 (1)	Ru1—Cl2	2.4872 (1)
Ru1—Cl2	2.423 (2)	Ru1—Cl4	2.5142 (1)
S1—N2	1.670 (3)	S3—N9	1.8018 (1)
Complex 6			
Ru1—N1	2.059 (3)	Ru52—N32	2.0221 (1)
Ru1—C10	2.154 (4)	Ru52—C1	2.2186 (1)
Ru1—C11	2.166 (4)	Ru52—C2	2.2321 (1)
Ru1—C12	2.218 (3)	Ru52—C3	2.2242 (1)
Ru1—C13	2.175 (3)	Ru52—C4	2.2587 (1)
Ru1—C14	2.147 (4)	Ru52—C5	2.1966 (1)
Ru1—C15	2.194 (3)	Ru52—C6	2.2270 (1)
Ru1—Cl1	2.395 (1)	Ru52—Cl53	2.5115 (1)
Ru1—Cl2	2.422 (1)	Ru52—Cl54	2.4867 (1)
S1—N2	1.663 (4)	S1—N2	1.7970 (1)

<sup>a</sup> [Å].

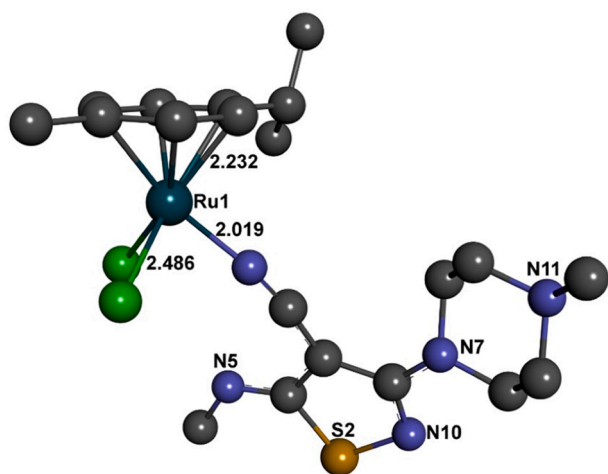


**Fig. 7.** DFT optimized structure of the complex **5** (hydrogen atoms were omitted having better clarity of picture).

increasing concentration of the compounds (Figs. S35–S40, ESI).

The addition of the ligands **1–3** and complexes **4–6** at diverse *r* values (Fig. 6) results in a decrease of the fluorescence intensity. This decrease of EB fluorescence (up to 30% of the initial CT-DNA-EB fluorescence intensity) suggests that they displace EB from the CT-DNA-EB complex so they can interact with CT-DNA probably by the intercalative mode [95].

The quenching parameters of ligands and complexes were calculated according to the Stern–Volmer equation (Eq. (3)) (see ESI) and are given in Table 5. The  $K_{SV}$  value was obtained from the slope in the plot of  $F_0/F$  versus [compound] (see inset in Figs. S38, S41 and S42, ESI). The complex **4** exhibits the lowest  $K_{SV}$  value (Table 5) and among all the compounds studied have the lowest ability to displace EB from its CT-DNA-EB complex. On the other hand, ligand **1** has the highest  $K_{SV}$  value and the greatest ability to displace EB from its CT-DNA-EB complex.

As can be seen from Table 5, the values of  $K_q$  were greater than  $10^{10} \text{ M}^{-1} \text{ s}^{-1}$ , indicating that the quenching mechanism, as a result of the formation of the CT-DNA-EB-compound complex, is a static quenching process.

### 3.6. Computational chemistry

The structure of isothiazole ligands and corresponding Ru(II) complexes have been solved by the X-ray analysis (an exception is complex **5** with piperazine substituent). This fact allowed us to compare their experimental structural properties with the results of density functional theory (DFT) calculations.

For this purpose, we carried out the geometry optimization of all ligands and their ruthenium(II) complexes starting from X-ray structures except for the complex **5** which has been modeled, preoptimized and then fully relaxed by the Gaussian. At first glance, the optimized structures are in good agreement with the experimental ones (Table 6). This means that the bonds, angles, and torsions fit well with X-ray findings except for slightly longer bonds (particularly in case of N–S bonds: 1.670 Å/DFT vs. 1.8018 Å/X-ray (complex **4**), 1.663 Å/DFT vs. 1.797 Å/X-ray (complex **6**)). DFT optimized structure of the unique unsolved complex **5** is given in Fig. 7, showing structural consistency with all the crystallographic structures.

#### 3.6.1. Docking

The study of metal–protein systems is of fundamental importance in biology, pharmacy, and medicine [96]. Covalent (coordinative) bonding (metalation) of Ru(II) piano stool complexes with proteins has been described by many authors [24]. Often these systems cannot be investigated through X-ray diffraction analysis, and other methods are necessary to characterize the structure and active site. The common spectroscopic and analytical techniques, such as NMR, EPR, ESEEM, ENDOR, ESI-MS, CD, and UV–Vis spectroscopy, often do not provide information on the region of the protein where the metal species are bound or on the amino acid residues involved in the coordination. Concerning the systems with covalent interactions, some authors recently tried to simulate the binding of small inorganic molecules to proteins, [97,98] but until now there were very few examples in which the docking methods have been systematically applied to the simulation of the covalent bonds between a protein and a metal species which, as mentioned above, represent most of the situations [66]. The method of Sciortino et al. [66] was thoroughly validated and results were always successful for 39 “pdb” structures, the pose with the highest affinity was the one suggested by the X-ray analysis; moreover, the crystallographic structure is reproduced with a success rate of 100% with an RMSD < 2.5 Å and of 90% with an RMSD < 1.5 Å [66].

We decided to check the interactions between our ligand and complexes against the two most abundant macromolecules HSA and DNA.

#### 3.6.2. HSA-L Covalent approach

HSA is an abundant plasma protein that binds a wide variety of hydrophobic ligands including fatty acids, bilirubin, and thyroxine. The GOLD suite was used for the study of HSA-Ligand docking. According to reported works on similar systems, we followed the next suggestions: docking on surface-exposed His-128, His-247, His-510 and Met-298 are denoted as coordination sites of Ru(arene) complexes [99].

Here we investigated the new GOLD docking method in the prediction of ruthenium(II)–HSA structures without using any geometrical constraints or energy restraints. In particular, our systems with ruthenium(II) metal-containing ligands were examined following the above findings and new coordination scoring parameters were generated. Following the results of kinetic studies that involve two HSA binding steps (associative slow and dissociative fast) we choose, at the first glance, the active species which were assumed on the basis of quantum mechanical thermodynamic parameters for the reactions given in Scheme 2.

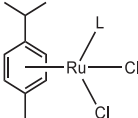
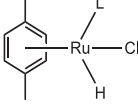
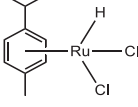
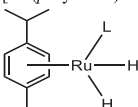
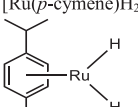
According to the results, we may assume that reactions 1. and 2. are very probable in protein surroundings and have been taken in the Gold docking process. Every leaving ligand has been replaced by hydrogen simulating bonding *d* orbital of ruthenium(II) (hydrogen acceptor). The



Hydrolysis		$\Delta G_{\text{react}}(\text{kcal mol}^{-1})$
1. $[\text{Ru}(\eta^6\text{-}p\text{-cymene})\text{-L-Cl}_2] + \text{H}_2\text{O} \longrightarrow [\text{Ru}(\eta^6\text{-}p\text{-cymene})\text{-L-Cl-H}_2\text{O}]^+ + \text{Cl}^-$		17.864716
2. $[\text{Ru}(\eta^6\text{-}p\text{-cymene})\text{-L-Cl}_2] + \text{H}_2\text{O} \longrightarrow [\text{Ru}(\eta^6\text{-}p\text{-cymene})\text{-Cl}_2\text{-H}_2\text{O}] + \text{L}$		6.553808
3. $[\text{Ru}(\eta^6\text{-}p\text{-cymene})\text{-L-Cl}_2] + 2\text{H}_2\text{O} \longrightarrow [\text{Ru}(\eta^6\text{-}p\text{-cymene})\text{-L-(H}_2\text{O)}_2]^{2+} + 2\text{Cl}^-$		45.549468
4. $[\text{Ru}(\eta^6\text{-}p\text{-cymene})\text{-L-Cl-H}_2\text{O}]^+ + \text{H}_2\text{O} \longrightarrow [\text{Ru}(\eta^6\text{-}p\text{-cymene})\text{-L-(H}_2\text{O)}_2]^{2+} + \text{Cl}^-$		27.684752
5. $[\text{Ru}(\eta^6\text{-}p\text{-cymene})\text{-L-(H}_2\text{O)}_2]^{2+} + \text{H}_2\text{O} \longrightarrow [\text{Ru}(\eta^6\text{-}p\text{-cymene})\text{-(H}_2\text{O)}_3]^{2+} + \text{L}$		6.001796
HSA		
6. $[\text{Ru}(\eta^6\text{-}p\text{-cymene})\text{-Cl}_2\text{-H}_2\text{O}] + \text{GLU}^- \longrightarrow [\text{Ru}(\eta^6\text{-}p\text{-cymene})\text{-Cl}_2\text{-GLU}]^- + \text{H}_2\text{O}$		23.75
7. $[\text{Ru}(\eta^6\text{-}p\text{-cymene})\text{-L-Cl}_2] + \text{GLU}^- \longrightarrow [\text{Ru}(\eta^6\text{-}p\text{-cymene})\text{-L-Cl-GLU}] + \text{Cl}^-$		-0.16
8. $[\text{Ru}(\eta^6\text{-}p\text{-cymene})\text{-L-Cl-H}_2\text{O}]^+ + \text{GLU}^- \longrightarrow [\text{Ru}(\eta^6\text{-}p\text{-cymene})\text{-L-Cl-GLU}] + \text{H}_2\text{O}$		-18.01
DNA		
9. $[\text{Ru}(\eta^6\text{-}p\text{-cymene})\text{-L-(H}_2\text{O)}_2]^{2+} + \text{GUA}^- \longrightarrow [\text{Ru}(\eta^6\text{-}p\text{-cymene})\text{-L-(H}_2\text{O)}\text{-GUA}]^+ + \text{H}_2\text{O}$		-20.46516253
10. $[\text{Ru}(\eta^6\text{-}p\text{-cymene})\text{-L-(H}_2\text{O)}_2]^{2+} + \text{GUA}^- \longrightarrow [\text{Ru}(\eta^6\text{-}p\text{-cymene})\text{-(H}_2\text{O)}_2\text{-GUA}]^+ + \text{L}$		-15.655412
11. $[\text{Ru}(\eta^6\text{-}p\text{-cymene})\text{-(H}_2\text{O)}_3]^{2+} + \text{GUA}^- \longrightarrow [\text{Ru}(\eta^6\text{-}p\text{-cymene})\text{-(H}_2\text{O)}_2\text{-GUA}]^+ + \text{H}_2\text{O}$		-21.657208

**Scheme 2.** Ru(II)-complexes hydrolytic reaction as well as their reactions with amino acids and nucleic bases involved in binding with HSA and DNA.

**Table 7**  
GOLD Docking results for reactive species of complex 4 within HSA molecule.

Molecule	Target	GoldScore	H-Bond	VdW	Closest
	Dom IIa (t1*)	49.3654	0.0000	49.5057	GLU292
	Dom IIIa (t2)	48.9523	0.4555	49.2984	SER489
	Dom IIIb (t3)	36.4380	0.0000	38.0773	THR506
	Dom IIIb (t4)	43.0681	0.0000	43.1599	PHE502
	Dom Ib (t5)	45.9801	0.6552	45.9044	LYS190
	Dom IIa (t1)	49.8461	0.3433	50.1322	GLU292
	Dom IIIa (t2)	49.2353	0.3462	49.5917	/
	Dom IIIb (t3)	36.7335	0.0000	40.6313	ILE513
	Dom IIIb (t4)	36.9874	0.0000	40.5804	ILE513
	Dom Ib (t5)	46.4044	0.0000	51.6866	ILE142
	Dom IIb	54.9454	2.0000	54.5788	LYS313
	Dom IIa (t1)	42.4609	14.4529	28.0733	GLU292
	Dom IIIa (t2)	34.0275	0.0000	34.0612	/
	Dom IIIb (t3)	35.7300	0.0000	36.3749	VAL555
	Dom IIIb (t4)	36.1986	0.0000	36.7017	VAL555
	Dom Ib (t5)	37.3229	0.0000	37.5151	ARG117
	Dom IIa (t1)	54.9402	7.2973	50.6794	GLU292
	HIS9	45.3104	0.0000	47.6583	ASP259
	HIS67	42.3003	0.0000	45.8937	HIS67
	HIS146	52.8325	0.0000	52.8325	HIS146
	HIS288	47.2563	0.0000	50.7460	LYS195
	HIS440	54.3591	0.0000	57.0849	ARG218
	Dom IIa (t1)	20.9078	0.0000	21.6449	LEU260
	Dom Ib (t5)	20.6208	0.2706	20.4924	GLU132

\*t1, t2, t3 and t4 denotes tyrosine bounded within 1HK1 molecule.

docking has been carried out on every active site of HSA and surface exposed cysteine and histidine. Our results are summarized in Table 7 and Fig. 8. It is more than clear that active species  $[\text{Ru}(p\text{-cymene})\text{LCl}(\text{H}_2\text{O})]^+$  and  $[\text{Ru}(p\text{-cymene})\text{Cl}_2(\text{H}_2\text{O})]$  are less active toward any histidine or cysteine but glutamine-292 being the common binding place in an associative mechanism of protein binding.

The results are indicative for HSA GLU-292 binding. Gold scores of  $[\text{Ru}(p\text{-cymene})\text{LClH}]$ ,  $[\text{Ru}(p\text{-cymene})\text{Cl}_2\text{H}]$  and  $[\text{Ru}(p\text{-cymene})\text{LH}_2]$  are the best scores of all reactive species. However, the last one appears to be a product of a dissociative step. Therefore our choice falls on the  $[\text{Ru}(p\text{-cymene})\text{LClH}]$  regarding to higher Gold score 49.8461 and a much higher VdW score 50.1322 than  $[\text{Ru}(p\text{-cymene})\text{Cl}_2\text{H}]$  species. More

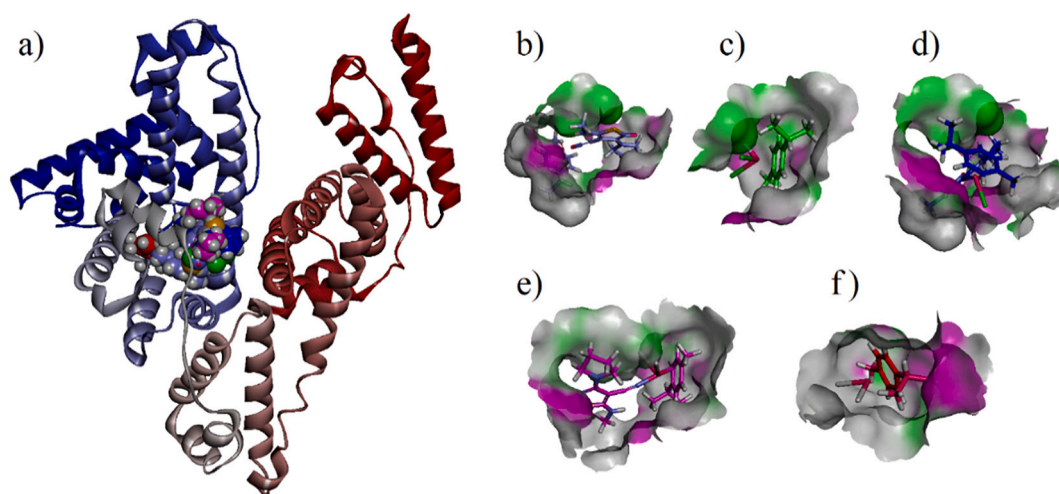


**Fig. 8.** (a) HSA with docked reactive species of complex 4, and orientations of docked conformations in domain IIA cavity for (b)  $[\text{Ru}(\text{p-cymene})\text{LClH}]$  (c)  $[\text{Ru}(\text{p-cymene})\text{Cl}_2\text{H}]$  (d) complex 4 (e)  $[\text{Ru}(\text{p-cymene})\text{LH}_2]$  and (f)  $[\text{Ru}(\text{p-cymene})\text{H}_2]$ .

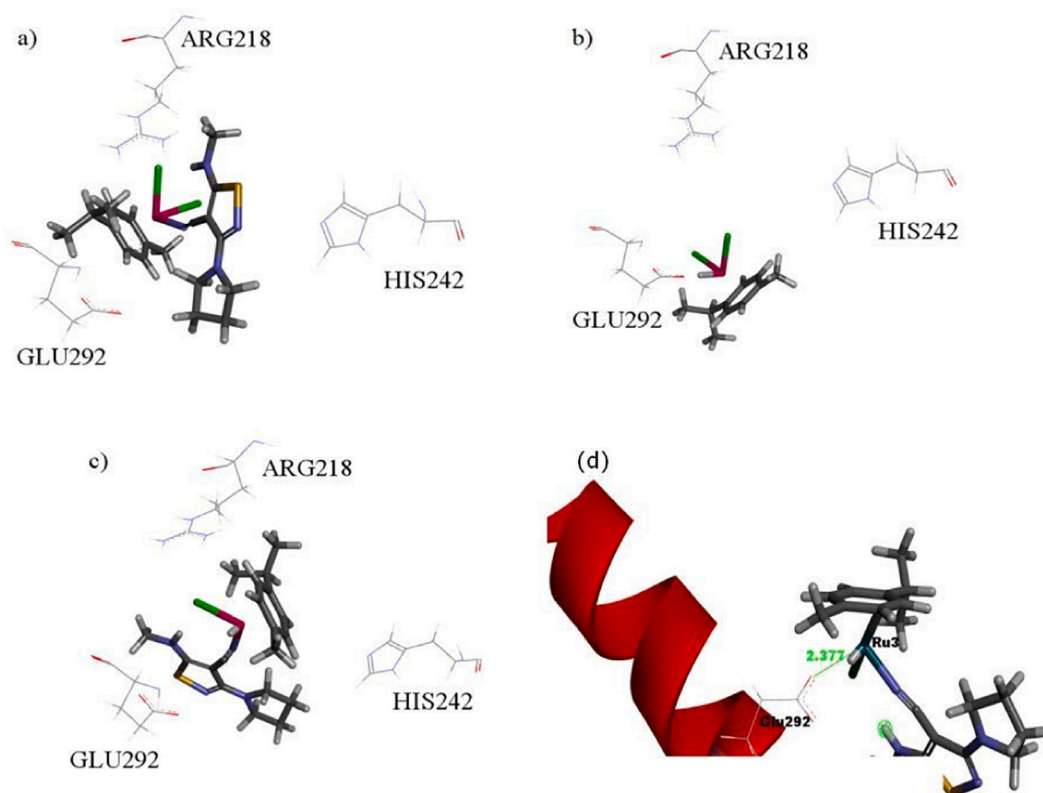


**Fig. 9.** Potential covalently binding residues inside cavity at the domain IIA of HSA with docked structures of reactive species of complex 4 (a)  $[\text{Ru}(\text{p-cymene})\text{Cl}_2\text{L}]$  (b)  $[\text{Ru}(\text{p-cymene})\text{Cl}_2\text{H}]$  and (c)  $[\text{Ru}(\text{p-cymene})\text{LClH}]$  (d) GOLD model as the Ru-H-O(GLU292) hydrogen bond interaction in case of (c).

important is the associative mechanism involving  $[\text{Ru}(\text{p-cymene})\text{LCl}_2]$  and HSA-GLU-292 account on chloride abstraction which is enough energy demanding to slow the binding process. Docked positions in relation to the residues that could potentially enter into covalent interactions inside the cavity of HSA at the IIA domain for complex 4 and some of the reactive species can be seen in Fig. 9.

The results of docking studies that involve first associative HSA binding step has been studied by the quantum mechanics as well (Scheme 2) and, one may see, given thermodynamic parameters for the exchange reactions, results are in accordance with our conclusion. This means that taking into account the first slow associative binding step of  $[\text{Ru}(\text{p-cymene})\text{LClH}_2\text{O}]^+$  to HSA and GOLD results (Fig. 9d) the second

fast reaction 7., appears to be very likely where neutral  $[\text{Ru}(\text{p-cymene})\text{LClGLU}]$  complex is formed according to high negative  $\Delta G_{\text{reaction}}$  value.

### 3.6.3. DNA

The above theory is indicative in terms of the formation of the protein-ligand complex. However, solution studies showed minimal spectral changes in the presence of HSA, implying small, or no rearrangement in the coordination sphere of Ru(II) ion. Therefore we can conclude that fast strong binding of the ligand/complex to HSA is thermodynamically less favored. This may lead us to conclusion that HSA actually has a transporter role at least within the timeframe of 48 h (according to kinetics experiments). One may expect for this prodrug to

**Table 8**

Docking results of  $[\text{Ru}(\eta^6\text{-p-cymene})\text{X}_2(\text{L})]$  ( $\text{X} = \text{Cl}$  or  $\text{H}_2\text{O}$ ) and different ligands toward DNA protein.

Compound	DNA		
	AutoDock		Vina
	$\Delta G^a$	$K_i^b$	Affinity <sup>a</sup>
1	-3.90	1.38 <sup>c</sup>	-5.30
2	-4.11	974.64	-5.60
3	-4.27	745.49	-5.70
4	-7.00	7.36	-7.10
5	-6.75	11.30	-7.50
6	-6.40	20.32	-6.90

<sup>a</sup> kcal mol<sup>-1</sup>.

<sup>b</sup> μM.

<sup>c</sup> mM.

**Table 9**

GOLD Docking results for complex 4 and reactive species with the DNA.

Molecule	GoldScore	H-bond	VdW	Closest
$[\text{Ru}(\text{p-cymene})\text{L}(\text{H}_2\text{O})\text{H}]$	46.89	7.80	41.55	dG7
$[\text{Ru}(\text{p-cymene})(\text{H}_2\text{O})_2\text{H}]$	37.50	10.00	29.66	dG7
$[\text{Ru}(\text{p-cymene})\text{H}_2]$	38.98	9.80	29.21	dG7
$[\text{Ru}(\text{p-cymene})\text{LH}_2]$	30.88	2.23	28.98	dG7
$[\text{Ru}(\text{p-cymene})(\text{H}_2\text{O})_3]$	30.04	0.00	30.12	dG7

enter cancer tissue and release a drug into the cell. Therefore it became of interest to investigate interactions of ligands with crucial cytoplasmatic macromolecule such as DNA.

Firstly two common docking software packages (parametrized Autodock and Vina) were used to reveal main interactions of DNA against all the prepared ligands and ruthenium analogues. Therefore, we have done a docking routine in the case of all the compounds using the procedure given in Experimental. Commonly established major

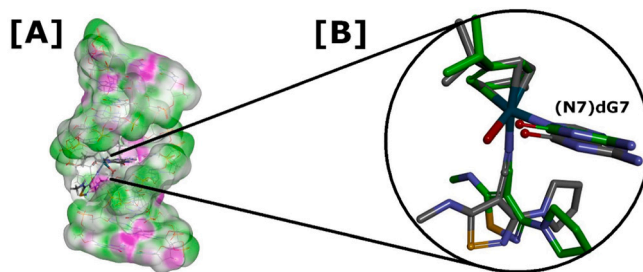


**Fig. 10.** [A] MOPAC-MOZYME PM6 optimized DNA/aquo complex of 4) structure of the best GOLD docking hit; [B] Overlay of MOPAC-MOZYME PM6 (green atoms) and QM (g09) optimized ruthenium(II) coordination sphere with RMSD = 1.051 Å.

**Table 10**

The IC<sub>50</sub> values of tested compounds and cisplatin.<sup>a</sup>

Samples	Cell lines				
	MRC-5	A549	MCF-7	HeLa	HT-29
1	>100	90.25	>100	>100	>100
2	>100	>100	25.64	45.3	>100
3	>100	89.07	7.04	>100	42.48
4	>100	32.46	6.34	>100	>100
5	>100	18.15	7.98	31.45	>100
6	>100	28.14	13.59	5.94	51.73
cis Pt	1.48	6.75	11.6	1.77	15.9

<sup>a</sup> [μM].

groove binding inside the DNA has been found as the best binding site in the case of all ligands and corresponding complexes. The results of the best hits are given in Table 8.

Evidently, the data given in Table 8, supports the hardest binding to DNA in the case of complex 4, which agrees with the solution study. The general positions of the ligands found inside the DNA major groove along with principal interactions are given in Fig. S43 (see ESI).

Natively Gold has been built up for protein-ligand interactions. Nevertheless, here we have used GOLD with the same modified parameter file [66] to dock ligands to the DNA dodecamer (as given in Experimental). For this experiment we have used several possible active species for which it might be reasonable to expect to form by hydrolytic processes inside of the cell (Scheme 2). The results of these docking experiments (GoldScore fitness, H-bond and VdW indexes) are given in Table 9. One may see that  $[\text{Ru}(\text{p-cymene})\text{L}(\text{H}_2\text{O})\text{H}]$  species has a highest GoldScore (46.89) and VdW index (41.55) with pretty high H-Bond index (7.80). This implies that this species is very likely when it comes to the covalent binding of ruthenium(II) complexes to DNA. Naturally, caution must be taken into account here because full parameterization of GOLD in the case of docking to the DNA has not been done.

To check the best docked conformation of  $[\text{Ru}(\text{p-cymene})\text{L}(\text{H}_2\text{O})\text{H}]^{2+}$  species we have used MOPAC [58] PM6-MOZYME method to optimize whole DNA/Ligand complex. The final solution is given in Fig. 10 which demonstrate the covalent bonding of Ru(II) and N(7) of dG7 nucleotide. This complex, that comprehends just guanine from dG7, was further QM optimized giving structure very similar to the one obtained by MOZYME (Fig. 10).

### 3.7. Biological tests

Based on the IC<sub>50</sub> value (Table 10), it is seen that the most sensitive cell lines to the effects of the tested substances were MCF-7, then A549 and HeLa, while the least sensitive were HT-29 cells. The MCF-7 cell line is the most sensitive to all of the tested compounds (except 1). In this case 3, 4 and 5 were about two times more active than cisplatin,

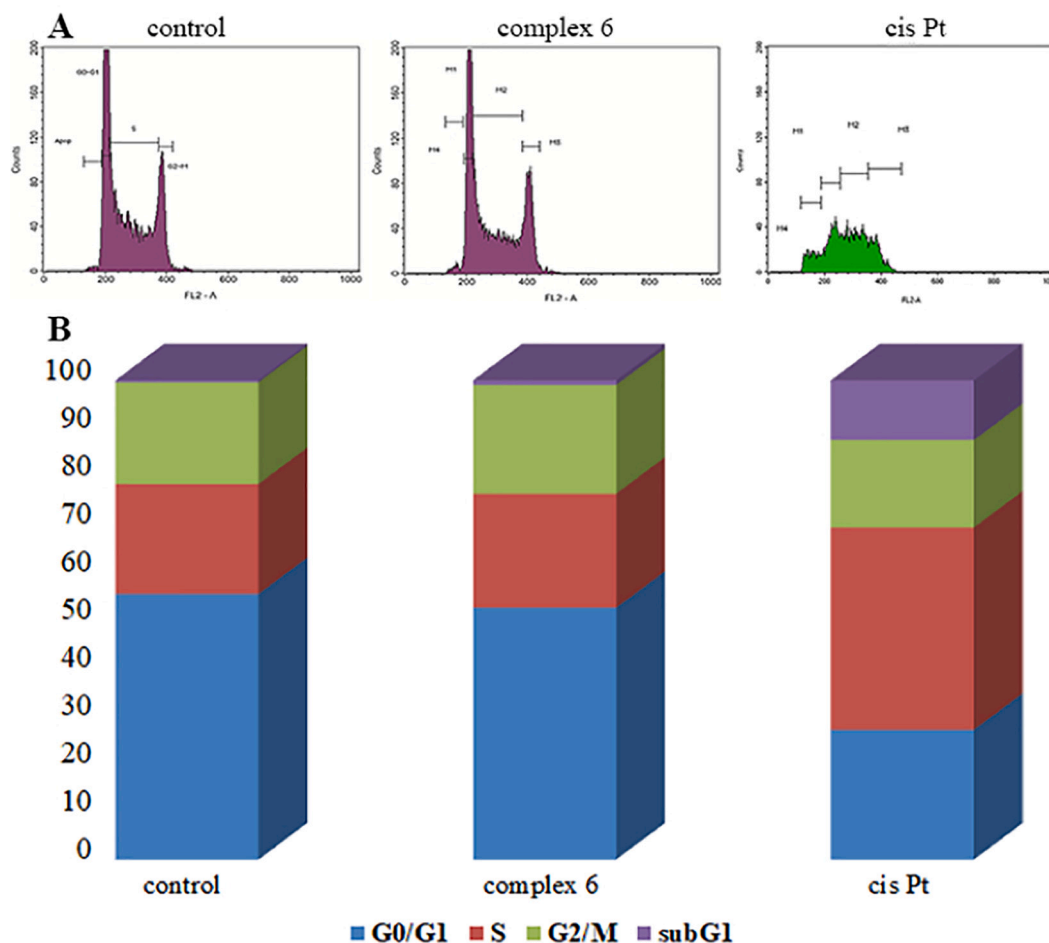


**Fig. 11.** Cell cycle analysis. (A) Histograms and (B) graph presenting cell cycle distribution in treated HeLa cells through the different cell cycle phases after 48 h exposure to the equitoxic doses ( $IC_{50}$  concentrations) of the tested complex **6** and cisplatin (cis Pt), along with untreated control sample.

while the antiproliferative activity of **6** was almost the same as with cisplatin. The tested compounds did not inhibit the growth of the HT-29 cell line, while the reference compound cisplatin exhibited a strong antiproliferative activity. Regarding the healthy MRC-5 cell line, the tested compounds were not toxic, only for the reference compound was shown to have significant activity.

The cell cycle of HeLa cells was examined using flow cytometry to determine the antiproliferative effect of synthesized substances. Complex **6** and cisplatin, after a 48-h treatment, reduced the percentage of cells in the G2/M phase by 40% and 10% relative to control, respectively. Complex **6** and the reference compound reduced the percentage of cells in the G0/G1 phase. Only cisplatin increases the percentage of cells in the S phase, compared to the control sample. After exposure of HeLa cells to complexes for 48 h, it was found that complex **6** and cisplatin increase the percentage of apoptotic cells (subG1 phase, Fig. 11). Flow cytometric analysis of Annexin-V-FLUOS stained cells showed that both complex **6** induces apoptosis in HeLa cells (Fig. 12). After 48 h treatment, the majority of cells were apoptotic (early apoptotic 7.23% and late apoptotic 8.8%), while only a small percent of cells was necrotic.

Also, the apoptotic response, shown as a percentage of specific apoptosis (Fig. 12), shows that cisplatin multiplies the percentage of HeLa cells that are positive for Annexin-V compared to the tested complex. The percentage of specific apoptosis of complex **6** is 13.36%. These results are in correlation with the results of the cell cycle analysis. The percentage of specific necrosis after 48 h for complex **6** is twice as high as in the reference compound.

#### 4. Conclusion

Three new  $[Ru(\eta^6\text{-}p\text{-cymene})Cl_2(L)]$  complexes with different substituted isothiazole ligands:  $[Ru(\eta^6\text{-}p\text{-cymene})Cl_2(L1)] \cdot H_2O$  (**4**),  $[Ru(\eta^6\text{-}p\text{-cymene})Cl_2(L2)]$  (**5**) and  $[Ru(\eta^6\text{-}p\text{-cymene})Cl_2(L3)]$  (**6**) were isolated and characterized using experimental and computational techniques. Crystal structures of three ligands and two complexes (**4** and **6**) have been verified by X-ray diffraction analysis. The interactions of CT-DNA and HSA with ligands and new ruthenium(II) complexes have been studied through absorption and fluorescence measurements. The high value of the binding constants,  $K_b$ , and the Stern–Volmer quenching constant,  $K_{SV}$ , is the result of good binding of complex **4** for CT-DNA and HSA. Docking experiments toward DNA dodecamer and HSA have been done. Kinetic studies on HSA–Ligand interaction suggest an associative manner that includes the replacement of labile aqua (or chlorido) ligand by protein donor to the metal center. The revised GOLD docking results are indicative for  $Ru(p\text{-cymene})Cl_2(L1)$  binding. Gold docking scores are in accordance with the associative mechanism involving  $[Ru(p\text{-cymene})Cl_2(L1)]$  and HSA-GLU-292 that rely on chloride abstraction which is high enough to slow the binding process. The same EES was used to dock ligands to the DNA dodecamer giving major groove binding of ligands as the principal ones. MOPAC-MOZYME optimization of the whole system of the best docked complex and QM relaxation of the initial ruthenium(II) coordination sphere are indicative for  $Ru(II)\text{-}N(7)dG7$  covalent binding. The results of biological tests showed that the ligands and new  $Ru(II)$  complexes in comparison to the reference compound cisplatin, have more desirable cytotoxic activity and unlike cisplatin, they are selective



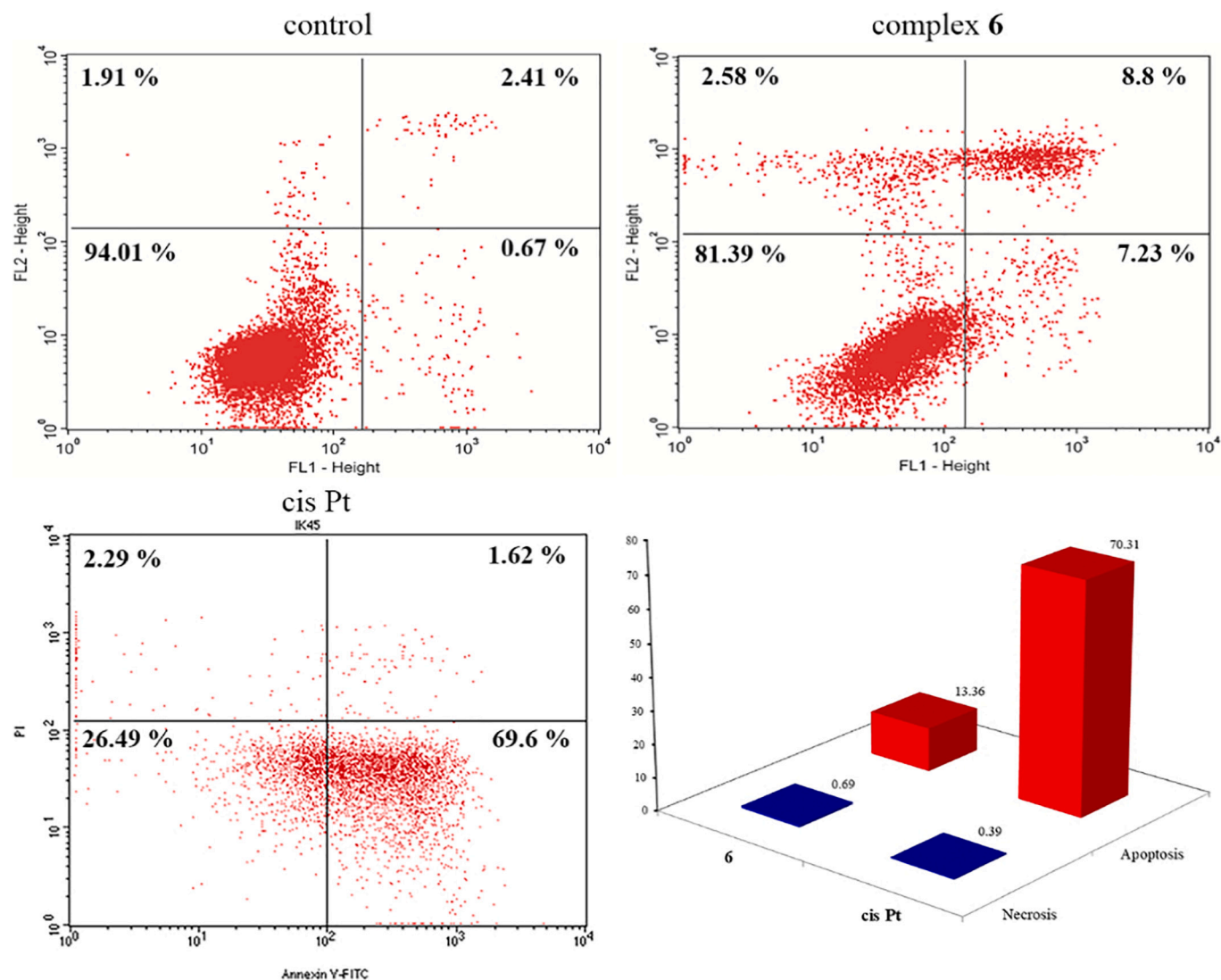


**Fig. 12.** Flow cytometric analysis of Annexin-V-FLUOS staining. Dot plots presenting the percentage of viable (lower left quadrant), early apoptotic (lower right quadrant), late apoptotic (upper right quadrant), and necrotic cells (upper left quadrant). Columns showing the percentage of specific apoptosis and specific necrosis of HeLa cells induced by cisplatin (cis Pt) and complex 6 after 48 h treatment. The percentage of specific apoptosis was calculated according to reference [71].

against cancer and healthy cell lines. For all the tested compounds results show that the MCF-7 cell line is the most sensitive. Flow cytometry analysis showed the apoptotic death of the cells with a cell cycle arrest in the subG1 phase.

#### Declaration of competing interest

The authors declare that they have no known competing financial interests or personal relationships that could have appeared to influence the work reported in this paper.

#### Acknowledgments

This work was supported by the Serbian Ministry of Education, Science and Technological Development (Agreement No. 451-03-68/2020-14/200122). The authors wish to thanks Dr. Giuseppe Sciortino and prof. Dr. Eugenio Garribba for their help in Gold software implementation, also we thanks prof. Dr. Biljana Petrović and Miss Milica Mededović for their help in kinetics' measurements.

#### Appendix A. Supplementary data

Crystallographic data are deposited in the Cambridge Crystallographic Data Centre as supplementary material number CCDC 1939949 - 1939953. Copies of this information may be obtained free of charge from the Director, CCDC, 12 Union Road, Cambridge, CB21FZ, UK (email: [deposit@ccdc.cam.ac.uk](mailto:deposit@ccdc.cam.ac.uk) or <http://www.ccdc.cam.ac.uk>). Supplementary data to this article can be found online at <https://doi.org/10.1016/j.jinorgbio.2020.111256>.

#### References

- [1] (a) B. Rosenberg, L. Van Camp, T. Krigas, *Nature* 205 (1965) 698–699; (b) B. Rosenberg, L. Van Camp, J.E. Trosko, V.H. Mansour, *Nature* 222 (1969) 385–386.
- [2] National Cancer Institute: Chemotherapy side effects sheets. [(accessed 2 May 2014)]; Available online: <http://www.cancer.gov/cancertopics/coping/physicaleffects/chemo-side-effects>.
- [3] W.H. Ang, P.J. Dyson, *Eur. J. Inorg. Chem.* 20 (2006) 4003–4018.
- [4] L. Zeng, P. Gupta, Y. Chen, E. Wang, L. Ji, H. Chao, Z.-S. Chen, *Chem. Soc. Rev.* 46 (2017) 5771–5804.
- [5] A. Sarkar, S. Acharya, K. Khushvant, K. Purkait, A. Mukherjee, *Dalton Trans.* 48 (2019) 7187–7197.
- [6] S.M. Meier-Menches, C. Gerner, W. Berger, C.G. Hartinger, B.K. Keppler, *Chem. Soc.*

- Rev. 47 (2018) 909–928.
- [7] A. Bergamo, C. Gaiddon, J.H.M. Schellens, J.H. Beijnen, G. Sava, *J. Inorg. Biochem.* 106 (2012) 90–99.
  - [8] C.S. Allardyce, P.J. Dyson, D.J. Ellis, S.L. Heath, *Chem. Commun.* (2001) 1396–1397.
  - [9] Z. Adhikarsan, G.E. Davey, P. Campomanes, M. Groessl, C.M. Clavel, H. Yu, A.A. Nazarov, C.H.F. Yeo, W.H. Ang, P. Dröge, U. Rothlisberger, P.J. Dyson, C.A. Davey, *Nat. Commun.* 5 (2014) 3462.
  - [10] Z. Mendoza, P. Lorenzo-Luis, M. Serrano-Ruiz, E. Martín-Batista, J.M. Padrón, F. Scalambra, A. Romerosa, *Inorg. Chem.* 55 (2016) 7820–7822.
  - [11] Z. Mendoza, P. Lorenzo-Luis, F. Scalambra, J.M. Padrón, A. Romerosa, *Dalton Trans.* 46 (2017) 8009–8012.
  - [12] Z. Mendoza, P. Lorenzo-Luis, F. Scalambra, J.M. Padrón, A. Romerosa, *Eur. J. Inorg. Chem.* (2018) 4684–4688.
  - [13] (a) F. Scalambra, P. Lorenzo-Luis, I. de los Ríos, A. Romerosa, *Eur. J. Inorg. Chem.* (2019) 1529–1538;  
(b) A. Guerriero, M. Peruzzini, L. Gonsalvi, *Coord. Chem. Rev.* 355 (2018) 328–361;  
(c) A. Rilak Simović, R. Masnikosa, I. Bratsos, E. Alessio, *Coord. Chem. Rev.* 398 (2019) 113011.
  - [14] S.H. van Rijt, P.J. Sadler, *Drug Discov. Today* 14 (2009) 1089–1097.
  - [15] N.P.E. Barry, P.J. Sadler, *Chem. Commun.* 49 (2013) 5106–5131.
  - [16] C.G. Hartinger, N. Metzler-Nolte, P.J. Dyson, *Organometallics* 31 (2012) 5677–5685.
  - [17] C.G. Hartinger, S. Zorbas-Seifried, M.A. Jakupec, B. Kynast, H. Zorbas, B.K. Keppler, *J. Inorg. Biochem.* 100 (2006) 891–904.
  - [18] S. Monro, K.L. Colón, H. Yin, J. Roque, P. Konda, S. Gujar, R.P. Thummel, L. Lilje, C.G. Cameron, S.A. McFarland, *Chem. Rev.* 119 (2019) 797–828.
  - [19] A. Bergamo, A. Masi, A.F. Peacock, A. Habtemariam, P.J. Sadler, G. Sava, *J. Inorg. Biochem.* 104 (2010) 79–86.
  - [20] L. Bíró, E. Farkas, P. Buglyó, *Dalton Trans.* 39 (2010) 10272–10278.
  - [21] L. Bíró, D. Huse, A.C. Bényei, P. Buglyó, *J. Inorg. Biochem.* 116 (2012) 116–125.
  - [22] Z. Bihari, Z. Nagy, P. Buglyó, *J. Organomet. Chem.* 782 (2015) 82–88.
  - [23] Z. Bihari, V. Ugone, E. Garribba, N. Lihi, P. Buglyó, *J. Organomet. Chem.* 823 (2016) 116–125.
  - [24] A. Merlino, *Coord. Chem. Rev.* 326 (2016) 111–134.
  - [25] E.S. Raper, *Coord. Chem. Rev.* 129 (1994) 91–156.
  - [26] E.S. Raper, *Coord. Chem. Rev.* 153 (1996) 199–255.
  - [27] E.S. Raper, *Coord. Chem. Rev.* 165 (1997) 475–567.
  - [28] H.R. Howard, J.A. Lowe III, T.F. Seeger, P.A. Seymour, S.H. Zorn, P.R. Maloney, F.E. Ewing, M. Newman, A.W. Schmidt, J.S. Furman, G.L. Robinson, E. Jackson, C. Johnson, J. Morrone, *J. Med. Chem.* 39 (1996) 143–148.
  - [29] M. Matsushita, N. Egashira, S. Harada, R. Okuno, K. Mishima, K. Iwasaki, R. Nishimura, M. Fujiwara, *J. Pharmacol. Sci.* 99 (2005) 154–159.
  - [30] T. Shiwa, T. Amano, H. Matsubayashi, T. Seki, M. Sasa, N. Sakai, *Jpn. J. Pharmacol. Sci.* 93 (2003) 114–117.
  - [31] L.M.T. Frija, A.J.L. Pombeiro, M.N. Kopylovich, *Coord. Chem. Rev.* 308 (2016) 32–55.
  - [32] A. Regiec, Z. Machon, R. Miedzybrodzki, S. Szymaniec, *Arch. Pharm.* 339 (2006) 401–413.
  - [33] Z. Machon, *Drugs Future* 13 (1988) 426–428 (and the references cited there).
  - [34] Z. Machon, A. Regiec, Z. Wiczorek, A. Potrykus, F. Przybylski, Register no. of patent notification 331778, Biuletyn Urzedu Patentowego (Bulletin of the Polish Patent Office (in Polish)) 18 (670) (1999) (Rok XXVII).
  - [35] N.A. Bumagin, S.K. Petkevich, A.V. Kletskov, V.I. Potkin, *Chem. Heterocycl. Compd.* 53 (2017) 1340–1349.
  - [36] N.A. Bumagin, V.M. Zelenkovskii, A.V. Kletskov, S.K. Petkevich, E.A. Dikumar, V.I. Potkin, *Russ. J. Gen. Chem.* 86 (2016) 68–81.
  - [37] R. Rivest, A. Weisz, *Can. J. Chem.* 49 (1971) 1750–1754.
  - [38] A.I.P. Sinha, J.L. Jain, B.K. Sinha, *Synth. React. Inorg. Met.-Org. Chem.* 14 (1984) 151–161.
  - [39] M. Đukić, M.S. Jeremić, R. Jelić, O. Klisurić, V. Kojić, D. Jakimov, P. Djurdjević, Z.D. Matović, *Inorg. Chim. Acta* 483 (2018) 359–370.
  - [40] J. Marmur, *J. Mol. Biol.* 3 (1961) 208–211.
  - [41] M.F. Reichmann, S.A. Rice, C.A. Thomas, P. Doty, *J. Am. Chem. Soc.* 76 (1954) 3047–3053.
  - [42] M.T. Cocco, V. Onnis, *Synthesis* (2013) 199–201.
  - [43] M.T. Cocco, C. Congiu, A. Maccioni, V. Onnis, M.L. Schivo, A. De Logu, *Il Farmaco* 49 (1994) 137–140.
  - [44] A.C. Vock, C. Scolaro, A.D. Phillips, R. Scopelliti, G. Sava, P.J. Dyson, *J. Med. Chem.* 49 (2006) 5552–5561.
  - [45] Oxford Diffraction, CrysAlis CCD and CrysAlis Red, Including SCALE3 ABSPACK, Oxford Diffraction, Abingdon, England, 2009.
  - [46] P. Coppens, F.R. Ahmed, S.R. Hall, C.P. Huber (Eds.), *Crystallographic Computing*, Munksgaard, Copenhagen, 1970, pp. 255–270.
  - [47] R.C. Clark, J.S. Reid, *Acta Cryst A* 51 (1995) 887–897.
  - [48] R.H. Blessing, An empirical correction for absorption anisotropy, *Acta Crystallogr. A* 51 (1995) 33–38.
  - [49] G.M. Sheldrick, *Acta Crystallogr. A* 71 (2015) 3–8.
  - [50] A.L. Spek, *J. Appl. Crystallogr.* 36 (2003) 7–13.
  - [51] L.J. Bruno, J.C. Cole, P.R. Edgington, M.K. Kessler, C.F. Macrae, P. McCabe, J. Pearson, R. Taylor, *Acta Crystallogr. B* 58 (2002) 389–397.
  - [52] L.J. Farrugia, *J. Appl. Crystallogr.* 32 (1999) 837–838.
  - [53] J.R. Lakowicz, *Principles of Fluorescence Spectroscopy*, 3rd edn, Springer, New York, USA, 2006.
  - [54] J.R. Lakowicz, G. Weber, *Biochem.* 12 (1973) 4161–4170.
  - [55] M.J. Frisch, G.W. Trucks, H.B. Schlegel, G.E. Scuseria, M.A. Robb, J.R. Cheeseman, G. Scalmani, V. Barone, B. Mennucci, G.A. Petersson, H. Nakatsuji, M. Caricato, X. Li, H.P. Hratchian, A.F. Izmaylov, J. Bloino, G. Zheng, J.L. Sonnenberg, M. Hada, M. Ehara, K. Toyota, R. Fukuda, J. Hasegawa, M. Ishida, T. Nakajima, Y. Honda, O. Kitao, H. Nakai, T. Vreven, J.A. Montgomery Jr., J.E. Peralta, F. Ogliaro, M. Bearman, J.J. Heyd, E. Brothers, K.N. Kudin, V.N. Staroverov, R. Kobayashi, J. Normand, K. Raghavachari, A. Rendell, J.C. Burant, S.S. Iyengar, J. Tomasi, M. Cossi, N. Rega, J.M. Millam, M. Klene, J.E. Knox, J.B. Cross, V. Bakken, C. Adamo, J. Jaramillo, R. Gomperts, R.E. Stratmann, O. Yazyev, A.J. Austin, R. Cammi, C. Pomelli, J.W. Ochterski, R.L. Martin, K. Morokuma, V.G. Zakrzewski, G.A. Voth, P. Salvador, J.J. Dannenberg, S. Dapprich, A.D. Daniels, O. Farkas, J.B. Foresman, J.V. Ortiz, J. Cioslowski, D.J. Fox, Gaussian 09, Revision D.01, Gaussian, Inc, Wallingford CT, 2013.
  - [56] Y. Zhao, D.G. Truhlar, *Theor. Chem. Accounts* 120 (2008) 215–241.
  - [57] (a) A. Bergner, M. Dolg, W. Kuechle, H. Stoll, H. Preuss, *Mol. Phys.* 80 (1993) 1431–1441;  
(b) M. Kaupp, P.V.R. Schleyer, H. Stoll, H. Preuss, *J. Chem. Phys.* 94 (1991) 1360–1366;  
(c) M. Dolg, H. Stoll, H. Preuss, R.M. Pitzer, *J. Phys. Chem.* 97 (1993) 5852–5859.
  - [58] MOPAC2016, J.J.P. Stewart, *Stewart computational chemistry*, Colorado Springs, CO, USA, <http://OpenMOPAC.net>, (2016).
  - [59] J. Řezáč, P. Hobza, *J. Chem. Theory Comput.* 8 (2012) 141–151.
  - [60] I. Petipás, C.E. Petersen, C. Ha, A.A. Bhattacharya, P.A. Zunsain, J. Ghuman, N.V. Bhagavan, S. Curry, *Proc. Natl. Acad. Sci. U. S. A.* 100 (2003) 6440–6445.
  - [61] M.S. Jeremić, M.D. Radovanović, F.W. Heinemann, M.M. Vasojević, Z.D. Matović, *Polyhedron* 169 (2019) 89–101.
  - [62] P.M. Takahara, A.C. Rosenzweig, C.A. Frederick, S.J. Lippard, *Nature* 377 (1995) 649–652.
  - [63] G.M. Morris, R. Huey, W. Lindstrom, M.F. Sanner, R.K. Belew, D.S. Goodsell, A.J. Olson, *J. Comput. Chem.* 30 (2009) 2785–2791.
  - [64] O. Trott, A.J. Olson, *J. Comput. Chem.* 31 (2010) 455–461.
  - [65] G. Jones, P. Willett, R.C. Glen, A.R. Leach, R. Taylor, *J. Mol. Biol.* 267 (1997) 727–748.
  - [66] G. Sciortino, J. Rodríguez-Guerra Pedregal, A. Lledós, E. Garribba, J.-D. Maréchal, *J. Comput. Chem.* 39 (2018) 42–51.
  - [67] J.D. Berić, S.D. Stojanović, E.M. Mrkalić, Z.D. Matović, D.R. Milovanović, M.M. Sovrić, R.M. Jelić, *Monatshefte für Chemie - Chemical Monthly* 149 (2018) 2359–2368.
  - [68] Y.N. Nosova, D.S. Karlov, S.A. Pisarev, I.A. Shutkov, V.A. Palyulin, M. Baquie, E.R. Milaeva, P.J. Dyson, A.A. Nazarov, *J. Organomet. Chem.* 839 (2017) 91–97.
  - [69] Dassault Systèmes BIOVIA, Discovery Studio, V.17.2.0, (2016).
  - [70] T. Mosmann, *J. Immunol. Methods* 65 (1983) 55–65.
  - [71] A. Bender, D. Opel, I. Naumann, R. Kappler, L. Friedman, D. Von Schweinitz, K.-M. Debatin, S. Fulda, *Oncogene* 30 (2011) 494–503.
  - [72] (a) K.N. Kumar, G. Venkatachalam, R. Ramesh, Y. Liu, *Polyhedron* 27 (2008) 157–166;  
(b) A. Juris, L. Prodi, A. Harriman, R. Ziesel, M. Hissler, A. El-hayoury, F. Wu, E.C. Riesgo, R.P. Thummel, *Inorg. Chem.* 39 (2000) 3590–3598;  
(c) J.V. Ortega, K. Khin, W.E. van der Veer, J. Ziller, B. Hong, *Inorg. Chem.* 39 (2000) 6038–6050;  
(d) R.N. Prabhu, D. Pandiarajan, R. Ramesh, *J. Organomet. Chem.* 694 (2009) 4170–4177;  
(e) J.M. Gichumbi, H.B. Friedrich, B. Omondi, *J. Organomet. Chem.* 808 (2016) 87–96.
  - [73] E.T. Peck, S. Hill, A.M. Williams, *Pharmacology for Anaesthesia and Intensive Care*, 3rd edn, Cambridge University Press, New York, 2008.
  - [74] Y. Wang, B. Tang, H. Zhang, Q. Zhou, G. Zhang, *J. Photochem. Photobiol. B Biol.* 94 (2009) 183–190.
  - [75] B.K. Sahoo, K.S. Ghosh, S. Dasgupta, *Biopolymers* 91 (2009) 108–119.
  - [76] B. Wu, M.S. Ong, M. Groessl, Z. Adhikarsan, C.G. Hartinger, P.J. Dyson, C.A. Davey, *Chem. Eur. J.* 17 (2011) 3562–3566.
  - [77] Y. Takezawa, P. Bockmann, N. Sugi, Z. Wang, S. Abe, T. Murakami, T. Hikage, G. Erker, Y. Watanabe, S. Kitagawa, T. Ueno, *Dalton Trans.* 40 (2011) 2190–2195.
  - [78] S.M. Meier, M. Hanif, Z. Adhikarsan, V. Pichler, M. Novak, E. Jirkovsky, M.A. Jakupec, V.B. Arion, C.A. Davey, B.K. Keppler, C.G. Hartinger, *Chem. Sci.* 4 (2013) 1837–1846.
  - [79] Protein Data Bank (<https://www.rcsb.org/>) PDB code: 4xuj. Accessed 3 July 2019.
  - [80] Z. Adhikarsan, G. Palermo, T. Riedel, Z. Ma, R. Muhammad, U. Rothlisberger, P.J. Dyson, C.A. Davey, *Nat. Commun.* 8 (2017) 14860.
  - [81] G.A. Davey, Z. Adhikarsan, Z. Ma, T. Riedel, D. Sharma, S. Padavattan, D. Rhodes, A. Ludwig, S. Sandin, B.S. Murray, P.J. Dyson, C.A. Davey, *Nat. Commun.* 8 (2017) 1575.
  - [82] M.P. Sullivan, M. Groessl, S.M. Meier, R.L. Kingston, D.C. Goldstone, C.G. Hartinger, *Chem. Comm.* 53 (2017) 4246–4249.
  - [83] W.H. Ang, L.J. Parker, A. Luca, L. Juillerat-Jeanneret, C.J. Morton, M.L. Bello, M.W. Parker, P.J. Dyson, *Angew. Chem. Int. Ed.* 48 (2009) 3854–3857.
  - [84] C.X. Zhang, S.J. Lippard, *Curr. Opin. Chem. Biol.* 7 (2003) 481–489.
  - [85] Q. Zhang, J. Liu, H. Chao, G. Xue, L. Ji, *J. Inorg. Biochem.* 83 (2001) 49–55.
  - [86] A.F. Tanius, D.Y. Ding, D.A. Patrick, C. Bailly, R.R. Tidwell, W.D. Wilson, *Biochemistry* 39 (2000) 12091–12101.
  - [87] Z.C. Liu, B.D. Wang, B. Li, Q. Wang, Z.Y. Yang, T.R. Li, Y. Li, *Eur. J. Med. Chem.* 45 (2010) 5353–5361.
  - [88] R.F. Pasternack, E.J. Gibbs, J.J. Villafranca, *Biochemistry* 22 (1983) 2406–2414.
  - [89] G. Prati, J. Bernadou, B. Meunier, *Adv. Inorg. Chem.* 45 (1998) 251–312.
  - [90] N. Lingthongambi, N. Rajen Singh, M. Damayanti, *J. Chem. Pharm. Res.* 3 (2011) 187–194.

- [91] M. Hazra, T. Dolai, A. Pandey, S. Kumar Dey, A. Patra, *Bioinorg. Chem. Appl.* 2014 (2014) 1–13.
- [92] D.Lj. Stojkovic, V.V. Jevtic, G.P. Radic, M.B. Đukic, R.M. Jelic, M.M. Zaric, M.V. Andjelkovic, M.S. Mistic, D.D. Baskic, S.R. Trifunovic, *New J. Chem.* 42 (2018) 3924–3935.
- [93] A. Dimitrakopoulou, C. Dendrinou-Samara, A.A. Pantazaki, M. Alexiou, E. Nordlander, D.P. Kessissoglou, *J. Inorg. Biochem.* 102 (2008) 618–628.
- [94] R. Sinha, M.M. Islam, K. Bhadra, G.S. Kumar, A. Banerjee, M. Maiti, *Bioorg. Med. Chem.* 14 (2006) 800–814.
- [95] W.D. Wilson, L. Ratmeyer, M. Zhao, L. Strekowski, D. Boykin, *Biochemistry* 32 (1993) 4098–4104.
- [96] D. Rehder, *Bioinorganic Chemistry*, Oxford University Press, Oxford, 2014.
- [97] G. Bianco, S. Forli, D.S. Goodsell, A.J. Olson, *Protein Sci.* 25 (2016) 295.
- [98] X. Ouyang, S. Zhou, C.T.T. Su, Z. Ge, R. Li, C.K. Kwok, *J. Comput. Chem.* 34 (2013) 326.
- [99] W. Hu, Q. Luo, X. Ma, K. Wu, J. Liu, Y. Chen, S. Xiong, J. Wang, P.J. Sadler, F. Wang, *Chem. Eur. J.* 15 (2009) 6586–6594.